energies

MDPI

Review

Switched Capacitor DC-DC Converters: A Survey on the Main Topologies, Design Characteristics, and Applications

Alencar Franco de Souza [1], Fernando Lessa Tofoli [2] and Enio Roberto Ribeiro [1,*]

[1] Institute of System Engineering and Information Technology, Federal University of Itajubá, Itajubá 37500-903, Brazil; alencar.souza@cefetmg.br
[2] Department of Electrical Engineering, Federal University of São João del-Rei, São João del-Rei 36307-352, Brazil; fernandolessa@ufsj.edu.br
* Correspondence: enio.k@unifei.edu.br

Abstract: This work presents a review of the main topologies of switched capacitors (SCs) used in DC-DC power conversion. Initially, the basic configurations are analyzed, that is, voltage doubler, series-parallel, Dickson, Fibonacci, and ladder. Some aspects regarding the choice of semiconductors and capacitors used in the circuits are addressed, as well their impact on the converter behavior. The operation of the structures in terms of full charge, partial charge, and no charge conditions is investigated. It is worth mentioning that these aspects directly influence the converter design and performance in terms of efficiency. Since voltage regulation is an inherent difficulty with SC converters, some control methods are presented for this purpose. Finally, some practical applications and the possibility of designing DC-DC converters for higher power levels are analyzed.

Keywords: DC-DC converters; integrated circuits; low-power electronics; semiconductors; switched capacitors

Citation: Souza, A.F.d.; Tofoli, F.L.; Ribeiro, E.R. Switched Capacitor DC-DC Converters: A Survey on the Main Topologies, Design Characteristics, and Applications. *Energies* **2021**, *14*, 2231. https://doi.org/10.3390/en14082231

Academic Editor: Ali Mehrizi-Sani

Received: 24 February 2021
Accepted: 7 April 2021
Published: 16 April 2021

1. Introduction

DC-DC converters are widely used in residential, commercial, and industrial applications, such as renewable energy conversion systems, electric traction devices, and, mainly, power supplies. Currently, it is estimated that more than 70% of electricity is processed by electronic devices [1]. In this context, increasing the power processing capacity and power density of converters associated with reduced manufacturing costs is of major concern.

The evolution of low-power electronics is mainly related to the increase in the purity of materials and advanced techniques used in the manufacture of integrated circuits (ICs) [2]. This also has a direct impact on power electronics, which seeks to increase the power levels and maximum operating frequency associated with reduced dimensions of power converters [3]. Recently, new semiconductors have become commercially available, which are based on silicon carbide (SiC) and gallium nitride (GaN). These elements have promising characteristics that allow the gradual replacement of silicon-based (Si) devices owing to their higher efficiency and operating frequency. Besides, there is the possibility of combining both manufacturing technologies in a single component [4–6].

In turn, energy storage devices such as capacitors and inductors, which are typically used as filters, also contribute directly to the improved performance of power converters. This is owing to the use of dielectric materials with optimized characteristics in capacitors [7,8]. Besides, new ferrosilicon alloys are capable of achieving higher magnetic permeability with reduced hysteresis and eddy current losses in the inductor cores [9–11].

In the constant search for higher power density in power converters, topologies using switched capacitors (SCs) have recently aroused the interest of industry and academia. These structures have been adopted in low power electronic applications, especially in systems with limited physical dimensions and involving high energy density. Their character-

istics allow monolithic integration [12,13], minimized levels of electromagnetic interference (EMI) [14–16], as well as reduced weight and volume.

However, despite the aforementioned advantages, these circuits may present low efficiency [17]. This aspect is particularly influenced by the intrinsic characteristics of the switches and capacitors used in the circuit, and the number of components must also be carefully considered [18]. The regulation of the load voltage is another challenge because, in certain operation conditions, the duty cycle does not have a linear relationship with the output voltage, which implies an increase in the complexity of the control systems [19].

SC circuits can also be combined with traditional structures based on inductors for obtaining families of hybrid converters, resulting in improved load voltage regulation and extended conversion ratio when compared with topologies composed only of capacitors and semiconductors [20,21]. An example of a pseudo SC bandpass filter can also be found in [22]. Another hybrid approach lies in resonant SC converters, which allow increasing the power processing capacity and power density as demonstrated in [23]. Considering that the combination of SCs and inductors leads to a wide variety of topologies, this analysis is beyond the scope of this work.

Considering that SC-based structures have inherent advantages and disadvantages, the existence of adequate guides that detail different design aspects for practical applications is of great interest to professionals and researchers. In this context, this work describes a synthesis of basic concepts and design guidelines associated with the conception of SC-based dc-dc converter topologies. Key issues such as classic configurations, semiconductors, efficiency, regulation, and operation modes are analyzed. The rest of the work is organized as follows. Section 2 addresses voltage multiplier circuits, as some SC cells are derived from these structures. Next, the SC DC-DC converters are presented. In turn, Section 3 is dedicated to analyzing the main design parameters, which includes the influence of components and operation modes in the converter efficiency, regulation, and control. Section 4 presents the main applications of these circuits, as well as future perspectives of their application. Section 5 summarizes the main aspects investigated in the study.

2. SC Structures

Although voltage multiplier circuits are simple structures widely known and described in analog electronics textbooks, they are still used in applications where high DC voltages must be obtained from an AC voltage source. Voltage multipliers are typically used in X-ray machines, scanning electron microscopes, and particle accelerators, among other devices, because they are simple and low-cost circuits [24–26].

In the literature, there are some SC structures dedicated to specific applications, which are often derived from basic converters [27–34]. A description of SC topologies and voltage multipliers used in the conception of non-isolated dc-dc converters for high step-up applications is presented in [35]. However, this study is specifically focused on the thorough analysis of existing techniques for extending the conversion range of non-isolated dc-dc converters. Some relevant issues for the design of SC-based converters are not addressed in [35], e.g., the proper choice of components, the charging mode of capacitors, evaluation of efficiency associated with relevant practical aspects, and control techniques aiming to achieve the output voltage regulation.

It is worth mentioning that there is a wide variety of circuits that employ inductors and SCs in the form of hybrid topologies, especially for wide conversion range applications [36–65]. Owing to the existence of a great diversity of combinations with distinct characteristics, this work is dedicated to the analysis of classical topologies based on the use of only semiconductors and capacitors, resulting in the so-called "pure SC" converters.

2.1. Greinacher Voltage Doubler (1914)

The simplest structure of a step-up converter that uses switches and capacitors is the Greinacher voltage doubler, which is shown in Figure 1 [66]. This circuit is powered by an

AC source and operates according to two stages. In the first one, the capacitor is charged to the peak value of the source voltage. In the second one, the previously charged capacitor is placed in series with the source and supplies a load. This combination generates a voltage that is ideally equal to twice the input voltage [67].

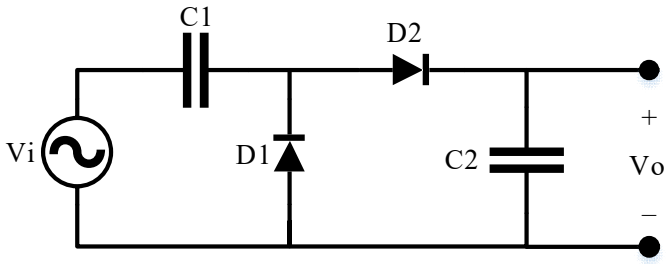

Figure 1. Greinacher voltage doubler.

Being a simple structure, this was one of the first topologies capable of stepping up the voltage across a load powered by an AC source using only passive semiconductors and capacitors. This circuit or cell can be connected in a modular way in series or parallel with phase opposition, thus allowing the achievement of high voltages [68,69].

2.2. SC Voltage Doubler

Although the voltage step-up circuit shown in Figure 1 may be useful in some applications, its use is only feasible when an AC voltage source is available. However, many electronic circuits are powered by DC sources. The SC voltage doubler (SCVD) circuit shown in Figure 2 is a suitable alternative in this case [70,71].

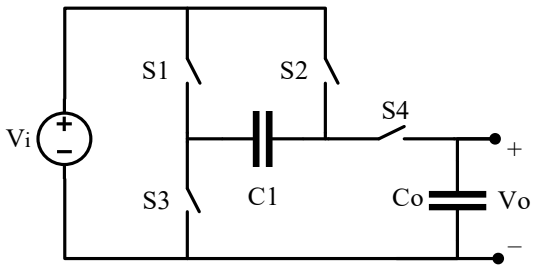

Figure 2. SCVD.

This structure employs active switches to control the charge and discharge of the capacitors. The circuit operates in the same way as the voltage multiplier, i.e., there are two stages. In the first one, the charge of capacitor C_1 occurs. In the second one, capacitor C_1 is connected in series with the source and the load. It is possible to employ the connection of several cells in series to obtain a given gain 2^n, where n is the number of associated stages. Thus, it is possible to obtain high voltage gains, which allow supplying loads with high output voltages.

2.3. Cockcroft Walton Voltage Multiplier or Ladder Structure (1932)

To supply a particle accelerator with a voltage of 1 MV, Cockcroft and Walton used a circuit powered by an AC source, substantially increasing the output voltage [72]. This circuit became known as Cockcroft and Walton voltage multiplier (CWVM), or simply voltage multiplier, which is exemplified in Figure 3 in terms of several stages. This is one of the best-known structures in electronics to obtain high gains owing to the simplicity of the circuit, low cost, and simple implementation. Considering the components as ideal, the output voltage V_o can be obtained by $n \cdot V_i$, where n is the number of associated cells and V_i is the input voltage.

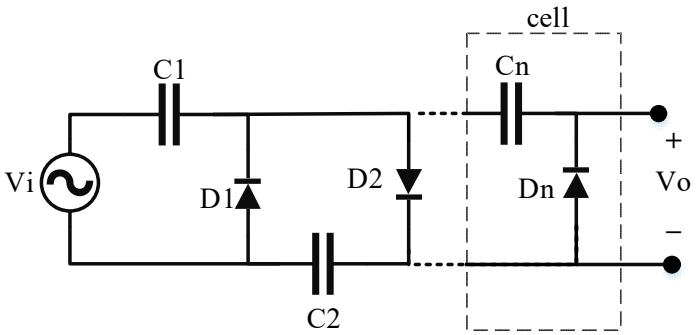

Figure 3. CWVM.

Recent works point to the possibility of using this structure in several modern applications involving high-gain DC-DC converters associated with photovoltaic modules [73,74] and even high power factor rectifiers [75–77].

In the CWVM, the source provides some charge Q to capacitor C_1 and, in each half cycle of the AC input voltage, the charge Q is transferred from capacitor to capacitor (C_2, C_3, ...), until it reaches the last element C_n. This process involves shifting the charge through each diode similarly to a ladder, which justifies the name given to the circuit.

An inherent problem with this topology is that its output impedance increases by an n^3 factor as the number of stages increases. This characteristic limits the output current to low values, as in the case of high currents; the output voltage will decrease rapidly owing to losses [78].

2.4. Series-Parallel Converter (1971)

A proposed alternative to overcome the main limitations of the CWVM in terms of voltage regulation is the series-parallel converter (SPC) shown in Figure 4 [79]. This converter is very versatile since each cell can be associated in series or parallel, and the output voltage can be modified at any time.

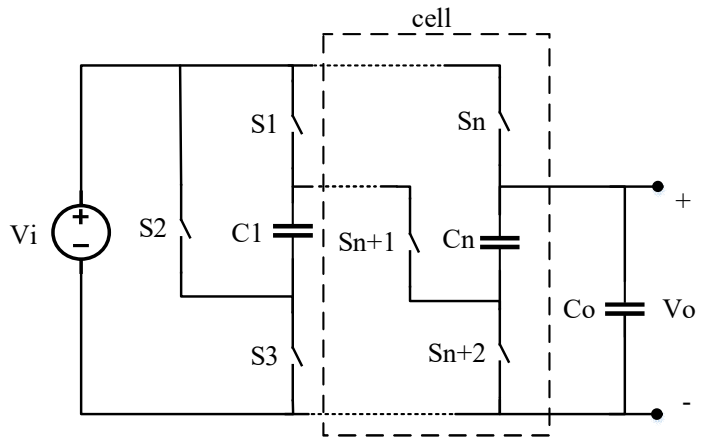

Figure 4. SPC.

As the name suggests, the energy transfer from the input to the output occurs when connecting some of the capacitors in parallel with the source during the charge stage. In a second moment, the capacitors are associated in series and supply the load. This arrangement has some remarkable advantages because it does not present the same problems as the CWVM, especially concerning the high output impedance. However, there are other drawbacks, such as the simultaneous charging of many capacitors, which can demand a high current from the source in a short time. Also, if many capacitors are in charging process, the voltage ripple at the output may be high, directly impacting the converter

efficiency. Depending on the length of the connection tracks on the printed circuit boards (PCBs), the arrangement of the elements, and the number of capacitors, there may still be problems due to parasitic capacitances, drastically reducing the efficiency of the circuit in the event of high voltage gains [80].

2.5. Series-Parallel Multiphase Converter (1973)

Another alternative to overcome the problems presented by the CWVM and the SPC is the series-parallel multiphase converter (SPMC) [81], which is shown in Figure 5. In this way, it is possible to mitigate the transients of the input current and the effect of parasitic capacitances. While part of the capacitors is connected to the source during the charge cycle, the other components that are fully charged are connected to the load. Meanwhile, part of the other series-connected capacitors remains in an intermediate charge state. Therefore, there are at least two or three phase-shifted signals controlling the connection of the capacitors with the source and the load.

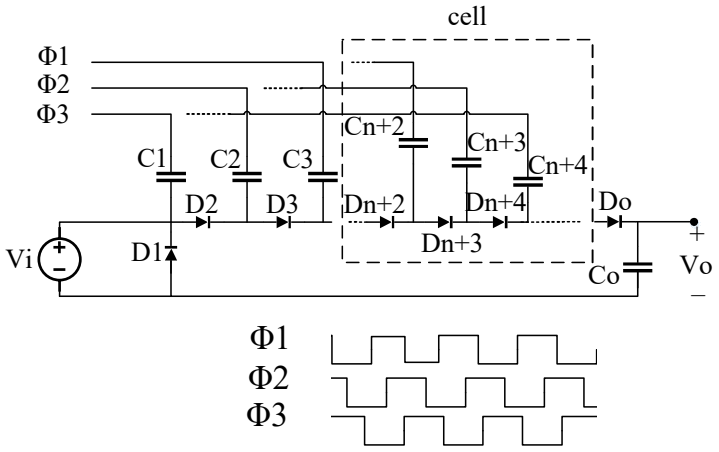

Figure 5. SPMC.

2.6. Dickson Converter (1976)

Dickson implemented the first integrated multiphase voltage multiplier in which the circuit reached an output voltage of 40 V from a 15 V source [82]. Besides the innovation inherent in the introduction of the topology itself, it should be noted that this was the first structure built experimentally in a totally encapsulated form. Figure 6 shows the Dickson converter.

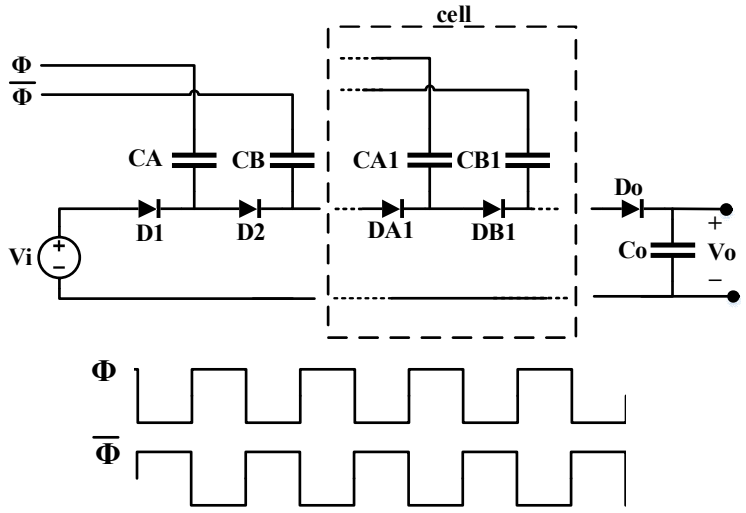

Figure 6. Dickson converter.

In the literature, there are several publications dedicated to the study of this topology aiming at improving aspects such as efficiency, dynamic response, and regulation [83–85]. A limitation of this structure lies in the fact that it does not present good performance in high-power applications owing to the difficulty of obtaining adequate regulation and the low efficiency when it is desired to obtain high voltage gains.

2.7. Fibonacci Converter (1991)

When the first SC converters were designed, the power levels were initially limited to milliwatts or a few units of watts. A natural next step would be to reduce the number of components of these structures, aiming at increasing the gain, power levels, and efficiency. In this sense, the Fibonacci converter (FC) was proposed as a multiphase topology in which the capacitors are associated in series and parallel. In this case, the cells are combined with the source and with each other to achieve the desirable voltage gain [86]. The FC is presented in Figure 7 and receives this name because of its gain characteristic, since each cell/stage coupled to the converter leads to an increase in the output voltage following a proportion defined by the Fibonacci sequence (2, 3, 5, 8, 13, . . .).

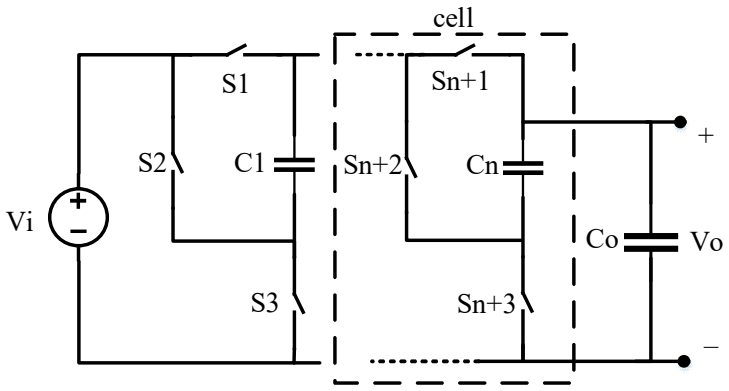

Figure 7. FC.

The FC is very similar to the SPC, differing mainly in the way the capacitors are connected. At this point, it should be noted that among the topologies presented so far that use the combination of capacitors in series and parallel, the highest gain by the association of stages is obtained with the FC [15,87].

2.8. Ladder Converter (1992)

The CWVM can produce high voltages from a low-voltage source, but there are limitations to this structure, such as the high output impedance that prevents high gains from being achieved. In general, it can be stated that as the gain increases, the output impedance also does by a cubic factor [79], which can compromise the output voltage regulation for loads requiring high currents.

The basic ladder cells are shown in Figure 8, which are derived from a study regarding the proposal of a three-level neutral point clamped (NPC) inverter topology [88,89]. The inverter described in [88,89] works with three voltage levels: V_i, $V_i/2$, and 0 V, and it is called capacitor-clamped multilevel inverter or flying capacitor multilevel inverter (FCMLI). This is a circuit similar to the NPC inverter, but the diodes are replaced by capacitors.

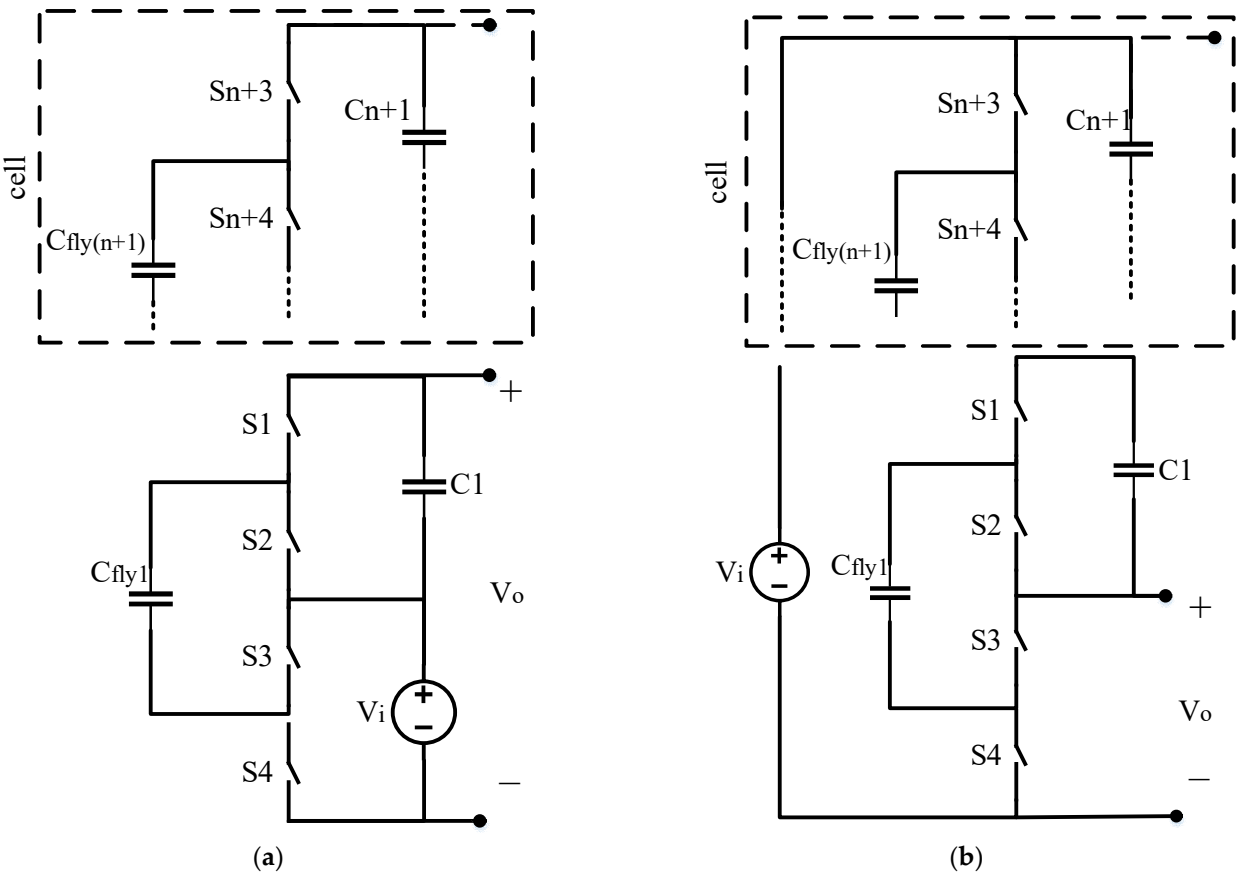

Figure 8. (**a**) Boost and (**b**) buck ladder cells.

These cells can be arranged in the form of boost and buck configurations as shown in Figure 8a,b, respectively. A converter based on this topology can consist of one or more cells according to the desired conversion ratio. When the converter works in voltage step-up mode, the source is associated in series with n capacitors charged with a voltage V_i. The flying capacitor at a given moment is connected in parallel with the source to be charged. Still, later it is connected in parallel with the other capacitor to charge it with V_i. In this way, the voltage source in series with n charged capacitors can produce an output voltage V_o according to Equation (1).

$$V_o = V_i + nV_i \tag{1}$$

when used as a step-down topology, the converter operates similarly to a capacitive voltage divider formed by n capacitors in series, in which the load is connected in parallel with one of the capacitors. In this circuit, there are also one or more flying capacitors C_{fly}, which at a given moment are connected in parallel with the source and later on associated in parallel with the elements that form the capacitive divider. This arrangement produces an output voltage that varies according to the number of capacitors used in the converter as defined by Equation (2):

$$V_o = \frac{V_i}{n_{cap}} \tag{2}$$

where n_{cap} is the number of series capacitors in the circuit. Figure 9a shows a boost-type ladder converter with a gain equal to two and Figure 9b presents a buck converter with a gain equal to 0.5. This topology is also efficient in AC-AC conversion, with good regulation and high power factor, and it is a feasible option to replace ferromagnetic core transformers [90].

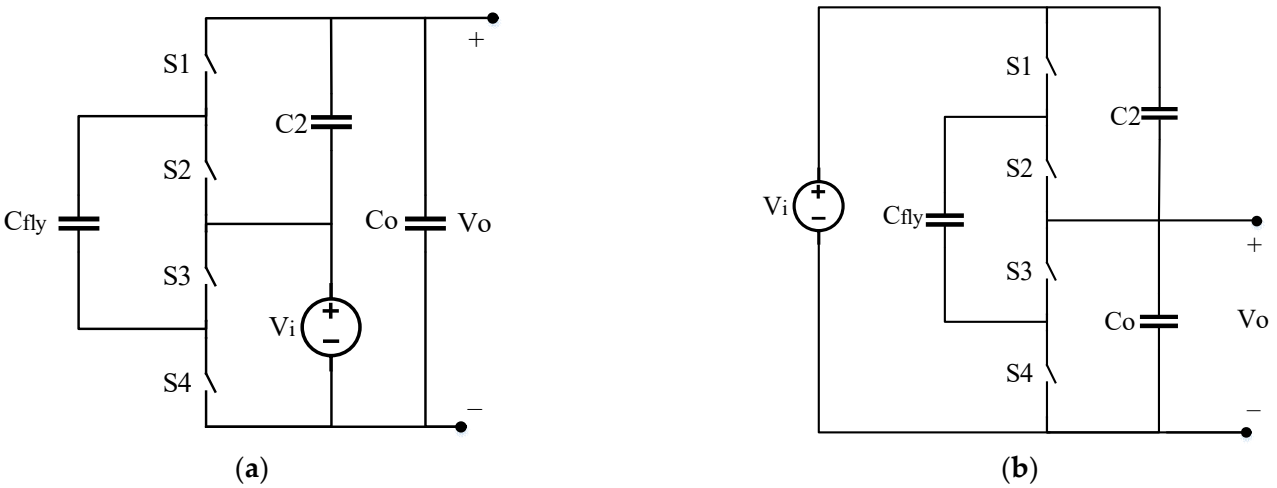

Figure 9. (**a**) Boost and (**b**) buck ladder converters.

3. Design Parameters

In this section, the main design parameters of SC converters are addressed, such as operation modes, main components, efficiency, and control techniques.

3.1. Components

3.1.1. Switches

In general, the efficiency and regulation of SC converters are dependent on the intrinsic resistances of the switches and the dielectrics that constitute the capacitors. In low-power and medium-power DC-DC converters, metal-oxide-semiconductor field-effect transistors (MOSFETs) are widely used because they can operate at high frequencies. For higher power levels, insulated gate bipolar transistors (IGBTs) are better recommend because they support higher currents and voltages, but switching losses increase significantly with the switching frequency. Some studies have shown that SiC MOSFETs have a performance similar to Si-based IGBTs [91–93]. Thus, the analysis presented in this work considers only MOSFETs.

Table 1 shows some characteristics of different commercial Si and SiC MOSFETs for comparison purposes. In these semiconductors, conduction losses must be carefully analyzed, as they depend on the drain-source on-resistance $R_{ds(\text{on})}$. This parameter is provided in the manufacturer's datasheet and expression 3 can be used to estimate the conduction losses [94,95]:

$$P_{cond(\text{MOSFET})} = R_{ds(on)} {I_{d(rms)}}^2 \tag{3}$$

where $I_{d(rms)}$ is the root-mean-square (RMS) drain current.

Table 1. Comparison of the characteristics of different MOSFETs.

Component	Type	$V_{ds(\text{max})}$ (V)	$I_{d(\text{max})}$ (A)	$R_{ds(\text{on})}$ (mΩ)	t_r (ns)	t_f (ns)	C_{oss} (pF)	C_{iss} (pF)
IRFP240	Si	200	20	180	51	36	400	1300
IRF530	Si	100	14	160	34	24	250	670
IRFP460	Si	500	20	270	51	36	430	1300
IRF840	Si	500	8	850	21	20	200	1225
C2M0080120D	SiC	1200	36	80	22	14	92	1130
SCT3080KL	SiC	1200	31	80	22	24	75	785
IMW120R045M1XKSA1	SiC	1200	52	59	24	13	115	1900
NTHL080N120SC1	SiC	1200	44	80	20	10	80	1112

The switching losses are essentially related to the time interval required by a given semiconductor to change from the ON state to the OFF state, or vice-versa. In other words, the shorter the rise time t_r and fall time t_f, the faster the dynamic response of a MOSFET. Table 1 shows the aforementioned parameters, as well as the parasitic capacitances that affect the switching losses. It is worth mentioning that C_{iss} and C_{oss} do vary significantly with the drain-source voltage V_{ds}, but they are only slightly affected by the temperature. Capacitance C_{iss} is an important parameter, since its charge and discharge are directly influenced by drive circuit connected to the gate. Besides, capacitance C_{oss} is charged by the voltage source of the circuit and discharged through the body diode when the MOSFET is ON and OFF, respectively.

In turn, the switching losses are calculated according to the energy dissipated in the switch during the turn-on and turn-off intervals. These losses depend on the switching frequency f_s, the drain-source voltage V_{ds}, the drain current I_d, and the time interval required for turn-on and turn-off of the transistor given by t_{on} and t_{off}, respectively. Thus, both parts are considered in expression (4) [96]:

$$P_{sw(\mathrm{MOSFET})} = \left(\frac{f_s V_{ds} I_d}{6}\right)\left(t_{on} + t_{off}\right) \tag{4}$$

Substituting the values assumed by distinct parameters defined in Table 1 in (3) and (4), it is observed that SiC MOSFETs present improved performance with respect to the conduction and switching losses when compared with their Si counterparts. Thus, SiC MOSFETs can be regarded as an adequate choice for applications that high conversion efficiency.

The transistors shown in Table 1 have good performance at high frequencies, but as the frequency increases, the switching losses can significantly compromise the efficiency of the converter. It is observed that the drain current also influences this behavior. As an example, Figure 10 represents the losses in a MOSFET model IRFP460 operating at 25 °C, subjected to a drain-source voltage of 100 V, while the switching frequency ranges from 0 to 500 kHz and, at the same time, the drain current varies from 0 to 10 A. This plot demonstrates the profile of losses in that particular component, but a similar analysis can be developed for any other commercial device, considering that its characteristics are provided by the manufacturer. Thus, one can consider these aspects in detail concerning the design and estimate of the converter efficiency.

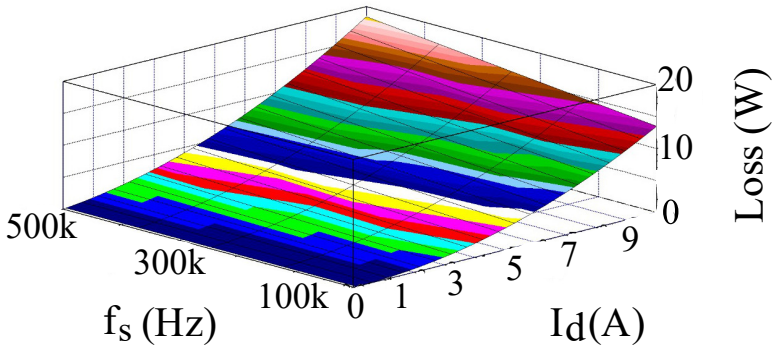

Figure 10. Behavior of switching and conduction losses in MOSFET IRFP460.

3.1.2. Diodes

Some SC topologies like Dickson, ladder, and SMPC use diodes besides active switches, which can influence the conversion efficiency significantly. Therefore, it is important to know the characteristics of such semiconductors, especially considering the commercial availability of Si and SiC components.

Table 2 summarizes the main parameters associated with some diode models, which include the maximum value of the repetitive peak reverse voltage V_{RRM}, the average

forward current $I_{F(\text{avg.})}$, the forward voltage drop V_F, the reverse recovery time t_{rr}, and the reverse recovery charge Q_{rr} as informed by the manufacturer at 25 °C. It is worth mentioning that the total capacitive charge Q_C of SiC diodes is equivalent to Q_{rr} in Si ones. Only ultrafast Si diodes are listed because SC converters often operate at high switching frequencies. Besides, only SiC Schottky diodes are described since this technology presents improved characteristics when compared with other solutions.

Table 2. Comparison of the characteristics of different diodes.

Component	Type	V_{RRM} (V)	$I_{F(avg.)}$	V_F (V)	T_{rr} (ns)	Q_{rr}/Q_C (nC)
MUR860	Si	600	8	1.20	60	195
RHRP8120	Si	1200	8	3.2	70	165
HFA15TB60S	Si	600	15	1.2	50	84
60EPU04	Si	400	60	1.05	85	375
IDT08S60C	SiC	600	8	1.5	-	20
C4D10120A	SiC	1200	33	1.5	-	52
SCS210KGHR	SiC	1200	10	1.4	-	34
IDH15S120	SiC	1200	15	1.65	-	54

SiC diodes are often much faster than Si ones and do not present significant problems due to the reverse recovery phenomenon, thus contributing to the reduction of switching losses. In either case, such semiconductors can be represented by the simple equivalent model shown in Figure 11, in which V_{to} represents the voltage drop across the semiconductor junction and r_t is the intrinsic resistance. The values of V_{to} and r_t are not often provided by manufacturers, even though they can be estimated from characteristic curves available in datasheets.

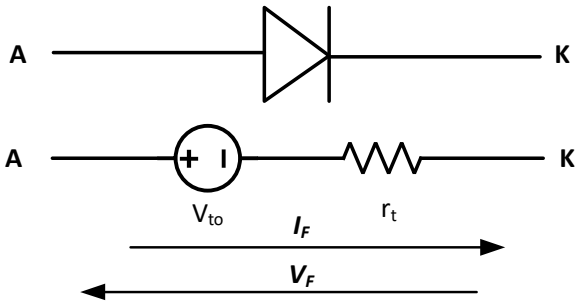

Figure 11. Diode symbol and equivalent model.

The aforementioned model can be used to estimate the losses in a diode. The conduction losses are owing to the current flowing through the component and can be calculated as in Equation (5).

$$P_{cond(D)} = V_{to} I_{F(avg.)} + r_t {I_{F(rms)}}^2 \quad (5)$$

where $I_{F(\text{avg.})}$ and $I_{F(\text{rms})}$ represent the average and RMS values of the forward current.

In turn, the switching losses occur during the turn-on and turn-off of the diode when both the current and voltage are not zero, being estimated from Equations (6) and (7), respectively.

$$P_{sw(on)(D)} = 0.5\left(V_{F(\max)} - V_F\right) I_{F(avg.)} t_{rr} f_s \quad (6)$$

$$P_{sw(off)(D)} = Q_{rr} V_{F(\max)} f_s \quad (7)$$

where $V_{F(\max)}$ is the maximum value assumed by the forward voltage drop. From Equation (6), it is observed that the longer t_{rr}, the higher the switching losses, and the lower the efficiency as a consequence. Besides, the efficiency can be further increased if diodes with low Q_{rr} or Q_C are chosen in practical designs.

3.1.3. Capacitors

Besides semiconductors, capacitors are essential devices in SC converters, as they are the only energy storage elements used in the circuit when hybrid topologies are not adopted, which also have inductors as in the case of [97]. The equivalent model of a capacitor basically consists of the series association of a capacitance C, the equivalent series resistance (ESR), and the equivalent series inductance (ESL) as shown in Figure 12.

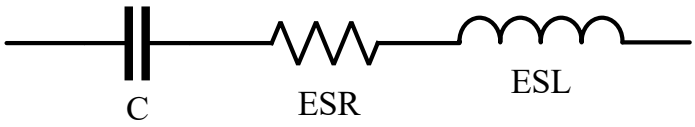

Figure 12. Equivalent circuit of a capacitor.

Capacitance *C* is related to the type of dielectric used in the construction of the component. It has a direct impact on the energy density and, consequently, on the dimensions of the converter. Parameter ESR cannot be accurately estimated from the simple measurement performed with an ohmmeter because it is strongly influenced by the dielectric, electrodes, and the ohmic losses in the terminals of the component.

The losses in dielectrics correspond to the delayed bias or relaxation, varying according to the dielectric medium, temperature, and frequency [98]. The losses in electrodes in low frequencies are essentially ohmic and depend on the dimensions and type of material. At high frequencies, the losses increase significantly owing to the skin and proximity effects.

Overall, it is reasonable to state that the losses in capacitors are influenced by a wide variety of aspects. In SC-based converters, this element can be satisfactorily represented by *C* and ESR, resulting in the representation shown in Figure 13. Parameter δ is called dissipation factor (DF) or loss angle, whose value is often provided in datasheets [99,100] In this way, it is possible to estimate the ESR using Equation (8) [101].

$$ESR = \frac{\tan(\delta)}{2\pi f_s C} \tag{8}$$

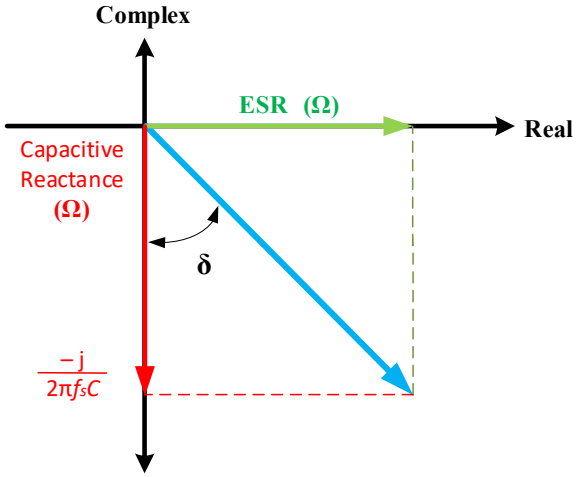

Figure 13. Representation of the loss angle of a capacitor.

The ESL can be hardly measured because it depends on the pad layout, capacitor height, and power plane spreading inductance [102]. It can be neglected at low frequencies, but its influence should be considered as the operating frequency gets close to the resonance frequency of the capacitor. The ESL limits the maximum switching frequency at which the converter can operate since, at very high frequencies, the inductive reactance is much

higher than the capacitive reactance. Figure 14 presents the behavior of the capacitor impedance as a function of the frequency and ESR [103].

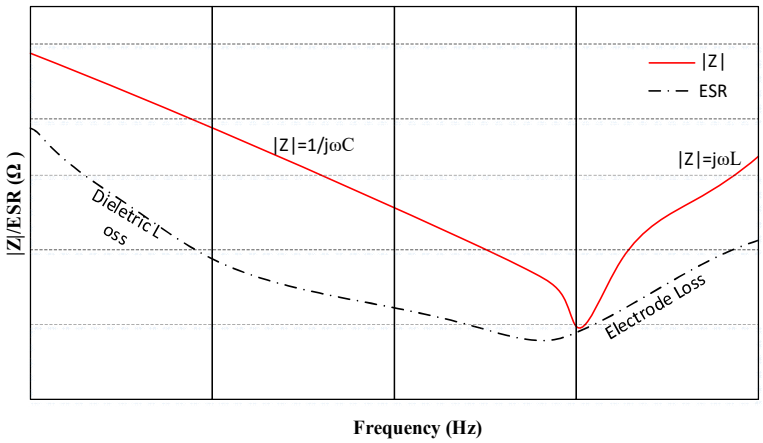

Figure 14. Behavior of the capacitor impedance as a function of the operating frequency and ESR.

Table 3 presents a comparison among eight commercially available capacitor models that use different types of dielectrics, which have a capacitance of 1 µF. Also, the maximum operating voltage varies according to the type of material used. An analysis is then performed considering important aspects such as volume, energy density, and the maximum loss angle measured at 1 kHz, so that the designer can be assisted in choosing the most adequate type of capacitor. The energy density has an impact on the size of the converter and, therefore, it is important to know how these parameters vary from one capacitor to the other according to the type of dielectric.

Table 3. Comparison among different types of capacitors.

Cap.	Manufacturer	Type	Series	V_{dc}	Vol. (mm^3)	E (mJ)	Dens. ($\mu J/mm^3$)	Max(tan (δ)) @1 kHz
1	Hitano	Electrolytic	ECR	47	215.98	1.25	5.78	0.10 *
2	Nichicon	Electrolytic	UMA	50	62.83	1.25	19.89	0.10 *
3	TDK	Polyester	B32560	63	244.8	1.98	8.10	0.008
4	Panasonic	Polyester	ECQE	100	1125.6	5	4.44	0.01
5	TDK	Polypropylene	B32672L	250	3663	31.25	8.53	0.0008
6	Hitano	Polypropylene	MKT	100	2592	5	1.92	0.01
7	TDK	Ceramic (ML)	FA24	50	67.5	1.25	18.51	0.03
8	Hitano	Ceramic (ML)	R25	50	132	1.25	9.46	0.1

* Value measured at 120 Hz as informed by the manufacturer.

The power dissipated in a capacitor depends on the root mean square (RMS) current $I_{C(\mathrm{rms})}$ and the ESR according to Equation (9).

$$P_{cap} = ESR \cdot {I_{C(rms)}}^2 \ (\mathrm{W}) \tag{9}$$

As the ESR depends on the DF and the frequency, it is possible to combine Equations (8) and (9) to approximately determine the losses in a capacitor according to Equation (10).

$$P_{cap} = \left[\frac{\tan(\delta)}{2\pi f_s C}\right] {I_{C(rms)}}^2 \tag{10}$$

As an example, and for the eventual efficiency analysis of the converters, capacitor 8 was chosen in Table 3. By varying the RMS current from 0 to 10 A and the source frequency

from 0 to 500 kHz, it is possible to plot the component losses as shown in Figure 15 with the aid of Equation (10).

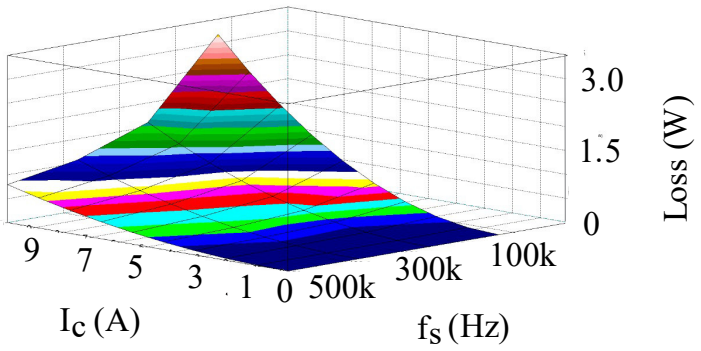

Figure 15. Behavior of losses in a capacitor as function of the RMS current and operation frequency.

Of course, each type of capacitor has its own electrical and constructive characteristics. The objective of this work is not to present a detailed analysis of these components, but only to address some important aspects that allow the choice of the most suitable element for a given application. In general, it is reasonable to state that the most popular capacitor used in SC converters is of film type. This component is widely used mainly in applications in which it is necessary to operate at high voltages and frequencies. The film dielectric has low DF, reduced ESR, and good response at high frequencies [104]. The dielectric consists of a thin layer of plastic, the most common materials being polyester and polypropylene. Capacitors made of metallized film have vaporized dielectrics with a thin layer of aluminum, as this additional layer provides the dielectric with the self-regeneration ability [105–107]. Given the possible occurrence of a voltage higher than the nominal value supported by the capacitor, which in turn would damage the dielectric, this characteristic allows rapid heating to occur owing to the short circuit of the plates. When subjected to high temperatures, this layer of aluminum around the hole turns into aluminum oxide, which has an insulating character and thus eliminates the short circuit.

Polyester capacitors can be found commercially from some units of nanofarads to values on the order of 220 µF, with voltages greater than or equal to 1000 V. This material often has limited use since, among the film-based capacitors, this is the type most sensitive to the increase of temperature [108] and frequency [104]. Its use is recommended mainly when it is desired to obtain converters with reduced dimensions since polyester capacitors have the smallest size for a given capacitance value in comparison to its remaining counterparts.

When compared to other components, polypropylene-based capacitors demonstrate excellent characteristics, such as the fact that the capacitance varies little with temperature, frequency, and voltage variations. Polypropylene absorbs less moisture than polyester, which makes this material suitable for a wide range of applications in harsh environments. Commercial capacitance values can reach up to 270 µF.

Ceramic capacitors are the passive devices most used in low power electronics today. In this case, the capacitance does not vary significantly with the frequency and temperature, while the components present low loss factor [109]. The dielectric materials used can be porcelain, mica, and other silicates. Also, the components can be produced on a single disc or in multiple layers, i.e., in the form of multilayer ceramic capacitors (MLCCs). A negative aspect lies in the fact that fractures in the dielectric can occur owing to voltage spikes and rapid changes in temperature, which can cause failures and even a short circuit in the capacitor [110]. These components are often manufactured with low capacitances, which are typically rated on the order of picofarads.

Within the most common commercial capacitors, the electrolytic capacitor has the most different construction characteristics. This element is formed by a sheet of porous paper embedded in an electrolyte and, to improve the contact of the plate with the welding terminal, the paper is wrapped in aluminum foil, so that this set forms the negative terminal

of the capacitor (cathode). The other terminal of the capacitor is connected internally to a second aluminum foil that constitutes the positive terminal (anode). This sheet receives an electrochemical treatment called anodic oxidation, which causes the appearance of a thin layer of an insulating material called aluminum oxide (Al_2O_3) deposited on that same sheet, thus forming the dielectric.

This Al_2O_3 oxide layer has the advantage of a high dielectric constant and high rigidity with a very thin thickness on the order of 0.7 µm. With this characteristic, it is possible to reach high capacitances in a very small volume, which can vary from 1 µF to 330 mF. Thus, this is one of the most important characteristics of this type of capacitor. On the other hand, the maximum voltage stresses supported by this component are low in relation to the other elements previously presented. If this type of component is subjected to transients that exceed the rated voltage, even if very briefly, the dielectric is compromised, causing a change in the capacitance value and reducing the component's useful life. In general, this type of capacitor has defined polarity and, if it is connected to a circuit in an inverted way, electrochemical reactions can occur inside it, causing leakage and even explosion. When high capacitances are required, their use is often essential, but these capacitors have a shorter useful life than film and ceramic components. As they are more susceptible to failure, their use on a large scale is avoided.

3.2. Operation Modes

As mentioned, SC converters have a simpler structure than conventional power electronic converters that employ inductors, but the control system becomes more complex in this case. Theoretically, it is possible to achieve high voltage gains with some structures. However, it should be noted that the higher the gain, the more components will be employed and, consequently, the lower the efficiency. Figure 16 presents the behavior of the theoretical voltage gain as a function of the number of cells for the voltage doubler, SPC, SPMC, Dickson, and FC topologies.

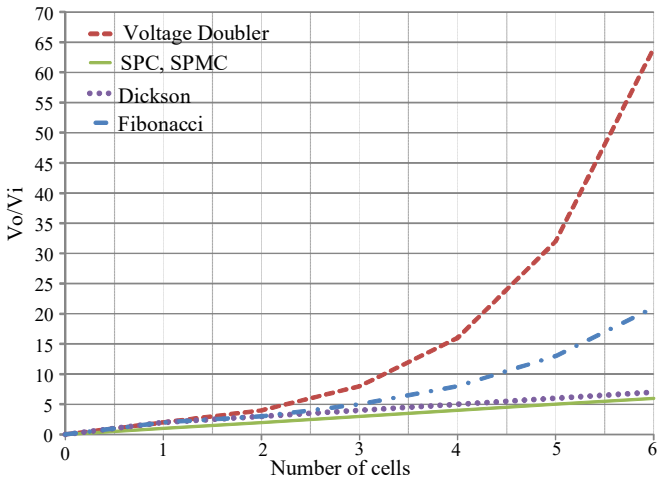

Figure 16. Behavior of the voltage gain of SC converters as a function of the number of cells.

To analyze the behavior of the output voltage, the circuit represented in Figure 17 is adopted. In this case, the converter can be modeled as an ideal transformer with turns ratio *m*:*n*, where R_o is the equivalent output resistance of the SC converter, which is connected in series with the load R_L [86,111]. In this model, the resistance R_o controls the power transferred to the load and the output voltage regulation. The variation of R_o in practice is mainly associated with the switching frequency and the internal resistance of the converter elements.

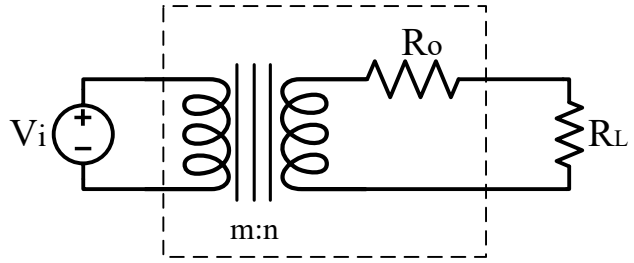

Figure 17. Simplified model used in the analysis of SC converters.

As for the switching frequency, two asymptotic limits can be established: slow switching limit (SSL) and fast switching limit (FSL) [112,113]. When the converter operates in SSL, the switching frequency is low enough for the capacitors to fully charge and discharge. In this scenario, the currents have short-term peaks. Besides, all resistances of the switches and capacitors are neglected, as these impedances do not affect the full charge of the capacitors. In this operation mode, the duty cycle has little influence on the behavior of the converter. In the FSL condition, the currents that flow through the capacitors can be considered constant, and the series resistances of the components cannot be neglected, as they can affect the full charge of the capacitors.

Other analytical methods are based on the charge and discharge of capacitors [114]. The circuit shown in Figure 18 can be used for this study, where an active switch S controls the energy transferred from a DC voltage source V_i to a capacitor C_o. This representation is simpler than the model corresponding to Figure 17 and leads to similar results, and is adopted in this work in the study of topologies. It addresses the behavior of the circuit according to three different modes shown in Figure 19, where the instantaneous voltage $v_{Co}(t)$ and instantaneous current $i_{Co}(t)$ are represented for the full charge, partial charge, and no charge conditions.

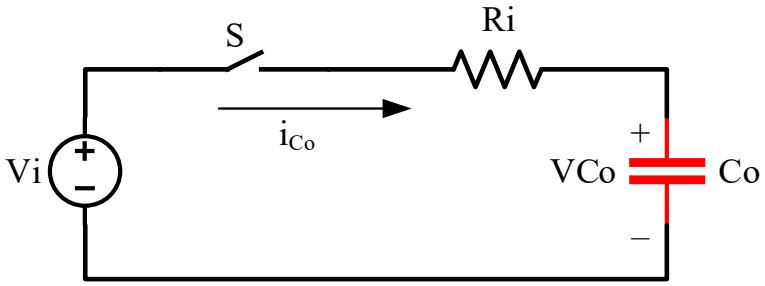

Figure 18. RC circuit used in the analysis of the charge and discharge of capacitors in SC converters.

In this case, the equivalent model of the converter is considered as a first-order R_iC_o circuit with time constant τ, where $R_i = R_{sw}$ + ESR, R_{sw} being the resistance of the switch, while C_o represents the capacitor in the charge or discharge regime. The switch is turned on to charge the capacitors during a time interval T_{on} over a switching period T_s. Thus, it is reasonable to state that SC circuits are often designed based on the time constant rather than the switching frequency. Besides, such converters are capable of operating in full charge condition even at high frequencies according to the specifications of capacitors and switches used in the design.

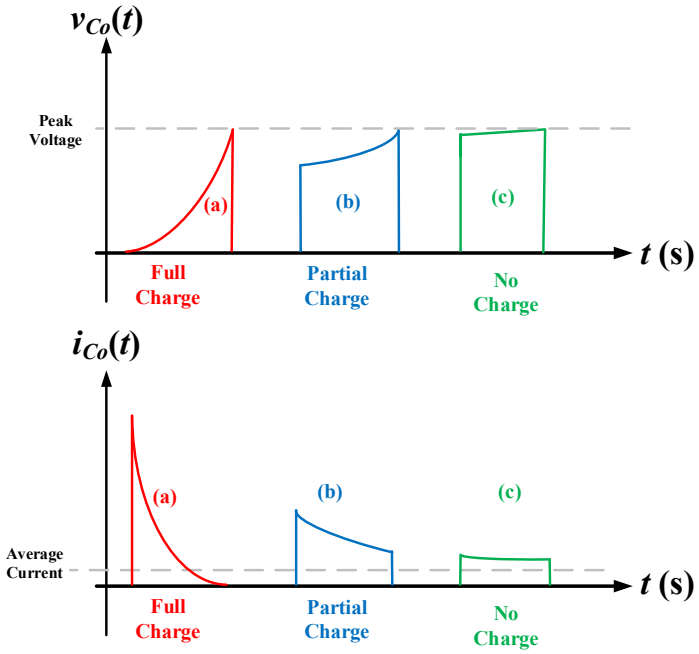

Figure 19. Capacitor charging modes: (**a**) full charge, (**b**) partial charge, (**c**) no charge.

The three modes of operation are defined [115,116]:

(1) If $T_{on} >> R_iC_o$, that is, when the time interval during which the switch remains on is much greater than the time constant of the circuit, the capacitors charge and discharge completely. Thus, the current becomes zero in each cycle, and then it can be assumed that the system operates under full charge condition according to Figure 19a.

(2) If $T_{on} \approx R_iC_o$, the capacitor current does not become zero and, therefore, the capacitor is not fully discharged [117]. The converter then operates on a partial charge condition. The representation of the current in the capacitor is shown in Figure 19b.

(3) If the switching frequency is very high, that is, if the value of T_{on} is small in relation to T_s, then $T_{on} << R_iC_o$. Thus, the current in the capacitor is almost zero, and the voltage across it can also be considered constant. In this mode, the converter operates at no charge condition according to Figure 19c.

In general, the equivalent resistance of the circuit represented in Figure 18 can be defined by Equation (11) [118]:

$$R_{eq} = \frac{1}{2f_sC_o}\frac{\left(1+e^{-\beta}\right)}{\left(1-e^{-\beta}\right)} \tag{11}$$

where β is given by Equation (12).

$$\beta = \frac{T_{on}}{R_iC_o} \tag{12}$$

The time constant associated with the circuit is given by Equation (13).

$$\tau = R_iC_o \tag{13}$$

The duty cycle is defined as the ratio between the on-time of the switch T_{on} and the switching period T_s as in Equation (14):

$$D = \frac{T_{on}}{T_s} \tag{14}$$

where T_s is defined according to Equation (15).

$$T_s = \frac{1}{f_s} \tag{15}$$

Defining $D = 0.5$, Expression (11) can be written as Expression (16).

$$R_{eq} = \frac{1}{2f_sC_o}\frac{\left[1 + e^{\left(-\frac{0.5}{\tau f_s}\right)}\right]}{\left[1 - e^{\left(-\frac{0.5}{\tau f_s}\right)}\right]} \tag{16}$$

Expression (16) is plotted in Figure 20a, where the behavior of the converter equivalent resistance is represented as a function of product $\tau \cdot f_s$. Proper tradeoffs must be made between such parameters to achieve good overall performance. Increasing the switching frequency may lead to higher efficiency as observed in Expression (16). However, it is worth mentioning that the switching losses and the existence of parasitic inductances and capacitances may affect the behavior of R_{eq} in practice, which tends to increase after a given point in the curve shown in Figure 20b [119]. Therefore, the efficiency will be reduced as a consequence. This condition depends on the characteristics of switches and capacitors used in the design, and such components must be wisely chosen in practical applications.

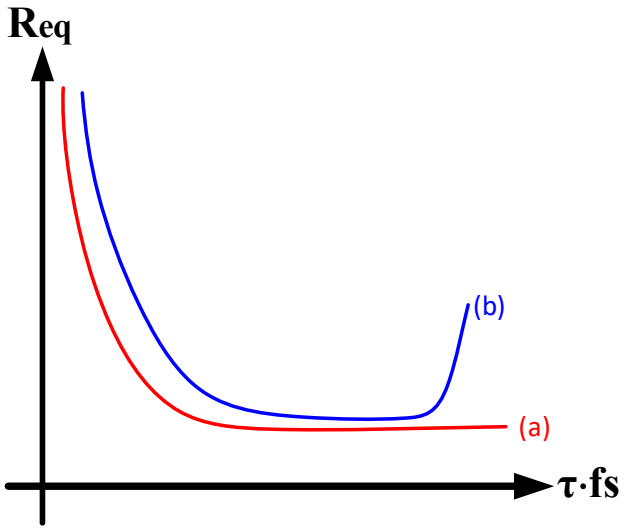

Figure 20. Behavior of the converter equivalent resistance as a function of the time constant and switching frequency: (**a**) ideal model; (**b**) real model.

Performing an analysis in terms of β and T_{on}, the output resistance of the converter can be estimated as follows:

(1) If $\beta > 1$, the converter operates in full charge mode, where $T_{on} > 5\tau$, while the output resistance depends on the inverse of the product of f_s and C_o. In other words, the resistances of the switches and capacitors represented by R_i has little influence on the converter behavior.

(2) If $\beta = 1$, the capacitors operate in partial charge mode and the output resistance of the converter depends on R_i, C_o, and f_s.

(3) If $\beta < 1$, the converter operates in no charge mode. In this case, it is possible to employ very short switching time intervals compared to the circuit time constant. Thus, the output resistance of the converter is very dependent on R_i and D.

Table 4 presents a comparison among the operation modes of SC converters.

Table 4. Operation modes of SC converters.

Operation Mode	Time Constant	β	Variation of R_{eq}
Full charge	$T_{on} >> R_i C_o$	$\beta > 1$	$\frac{1}{2f_s C_o}$
Partial charge	$T_{on} \approx R_i C_o$	$\beta \approx 1$	$\beta, \frac{1}{2f_s C_o}$
No charge	$T_{on} << R_i C_o$	$\beta < 1$	$R_i \frac{T_s}{T_{on}} = \frac{R_i}{D}$

3.3. Voltage Balance

SCs rely on the principle that the energy stored in a given element is transferred to another, while the capacitors can be associated in series or in parallel depending on the configuration. Of course, small differences will exist in the rated capacitances even if components with the very same specifications are used. In most SC converters, the energy transfer occurs in equivalent circuits represented by the parallel association of capacitors. A given capacitor C_i previously charged with a voltage V_{Ci} transfers energy to another capacitor C_o, which has no charge or a smaller amount of charge according to the circuit shown in Figure 21. It is worth mentioning that a given series resistance R_i also exists in practice owing to capacitors C_i and C_o, as well as to the active switches.

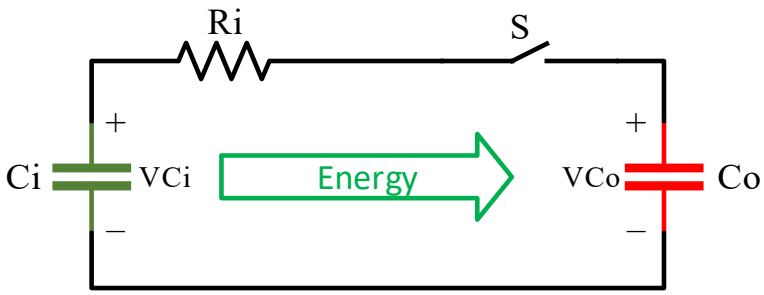

Figure 21. Circuit representing the energy transfer between two capacitors.

The series resistance is neglected a priori in the forthcoming analysis. Thus, the total amount of charge in the circuit Q_t is given by Equation (17):

$$Q_t = Q_{Ci} + Q_{Co} \tag{17}$$

where Q_{Ci} and Q_{Co} are the charges stored in capacitors C_i and C_o, respectively.

Since charge balance is supposed to occur, the initial charge Q_i must be equal to the final charge Q_f according to Equation (18).

$$Q_f = Q_i \tag{18}$$

Considering this condition, Expression (19) is valid:

$$V_{Ci}C_i + V_{Co}C_o = V_f C_i + V_f C_o \tag{19}$$

where V_{Co} is the initial voltage across capacitor C_o; and V_f is the final value assumed by the equilibrium voltage.

Thus, it is possible to obtain V_f from Expression (19) as in Expression (20).

$$V_f = \frac{V_{Ci}C_i + V_{Co}C_o}{C_i + C_o} \tag{20}$$

If C_o is initially discharged, then V_{Co} = 0 and Expression (19) becomes (21).

$$V_{Ci}C_i = V_f C_i + V_f C_o \tag{21}$$

Thus, Expression (22) results.

$$V_f = V_{Ci}\left(\frac{C_i}{C_i + C_o}\right) \tag{22}$$

The behavior of the voltages across the capacitors does depend on the charge mode as shown in Figure 19. On the other hand, the rated value of the equilibrium voltage achieved when one capacitor transfers charge to another depends on the capacitances, which may vary in practical conditions owing to distinct factors, e.g., aging, temperature, among others. If V_{Ci} remains constant while considering distinct combinations of C_o and C_i, it is observed that the equilibrium voltage changes when the capacitances are not the same. Another important issue is the fact that the value of R_i does not affect the value assumed by V_f, but only the time constant of the circuit. This aspect also becomes evident in Section 3.4, where it is demonstrated that R_i does not affect the conversion efficiency during the charge cycle.

3.4. Efficiency

There are many works dedicated to analyzing the variables that influence the efficiency of SC converters. Some studies point out the constructive characteristics of capacitors [120], the intrinsic resistance of switches [121], or even a combination of both as the main factors responsible for affecting this behavior [122]. Other aspects are also brought up, such as the voltage conversion ratio and the charge regime, that is, full charge or no charge [123].

As previously mentioned, in each cycle when in full charge mode, the capacitor discharges fully. For a circuit in which the capacitor is initially discharged, the maximum theoretical efficiency achievable is 50% according to Equation (23). As the initial voltage on the capacitor increases, the efficiency also does. The same behavior occurs when operating with partial charge, and the efficiency does not depend on the resistance of the switches and capacitors according to Equation (24). The charging process is affected only by the initial and final values of the capacitor voltage. Therefore, the greater the voltage variation, the lower the efficiency during the charge cycle. The increase of the resistances in series with the capacitors during the charge cycle only modifies the time constant, but it does not affect the efficiency itself. An increase in such series resistances during the charge cycle decreases the peak current and, at the same time, increases the charge time. Thus, the efficiencies under full charge and partial charge conditions are given by η_{FC} and η_{PC} in Equations (23) and (24), respectively.

$$\eta_{FC} = \frac{1}{2}\left(1 + \frac{V_{initial}}{V_i}\right) \tag{23}$$

$$\eta_{PC} = \frac{1}{2}\left(\frac{V_{initial} + V_{final}}{V_i}\right) \tag{24}$$

where $V_{initial}$ and V_{final} are the initial and final values of the capacitor voltage, respectively.

During the discharge cycles, the efficiency can be estimated in at least three different ways: capacitor discharging in a resistance; capacitor discharging into another capacitor; and capacitor discharging into a parallel RC circuit.

For the first case, the efficiency is given by (25):

$$n_R = \frac{R_L}{R_L + R_i} \tag{25}$$

where R_L is the resistance on which the capacitor is discharged. It is observed that the lower the series resistance, the higher the circuit efficiency. Thus, it is interesting to know the parameters presented in Tables 1 and 3.

However, for the capacitor discharge in another capacitor, the efficiency can be estimated in two ways that depend on the operation mode in which the circuit works, that is,

full charge or no charge. As an example, Figure 21 shows the circuit used in the analysis, whose waveforms in Figure 22 represent the moment after which switch *S* is turned on.

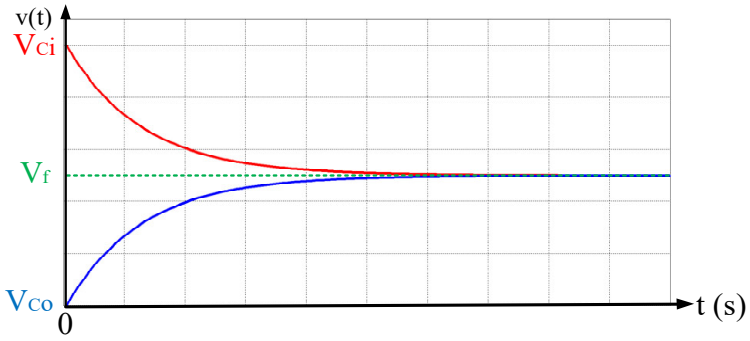

Figure 22. Waveforms representing the discharge of one capacitor into another capacitor in full charge mode.

As previously mentioned, capacitor C_i is initially charged with voltage V_{Ci}, whereas capacitor C_o is completely discharged. Thus, a charge balancing occurs so that at the end of the process, the voltage on both capacitors becomes nearly balanced and equal to $V_{Ci}/2$ if the capacitances are equal to each other. Therefore, the voltages across C_o and C_i are increased and decreased, respectively, as the efficiency can be calculated according to Equation (26).

$$n_{FC} = \frac{V_f + V_{Co}}{V_f + V_{Ci}} \tag{26}$$

Considering a capacitor discharging into another capacitor, but in partial charge mode, a similar analysis can be performed. Now, the capacitor C_i initially charged with V_{Ci} is discharged into another capacitor until reaching $V_{Ci(min)}$. In this way, the capacitor C_o charges from a minimum voltage V_{Co} to $V_{Co(\max)}$, and then the cycle is interrupted. The behavior of the capacitor voltages in this case is shown in Figure 23. The efficiency of this type of discharge cycle can be given by Equation (27):

$$n_{PC} = \frac{V_{Co(\max)} + V_{Co}}{V_{Ci} + V_{Ci(\min)}} \tag{27}$$

where $V_{Co(\max)}$ is the maximum voltages on capacitor C_o; and $V_{Ci(\min)}$ is the minimum voltage on capacitor C_i.

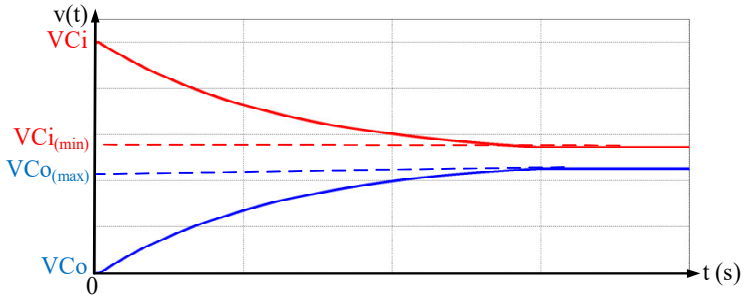

Figure 23. Waveforms representing a capacitor discharging into another capacitor in partial charge mode.

A third possibility is the discharge of a capacitor in a parallel RC circuit, as shown in Figure 24. In this case, there is a capacitor C_i charged with an initial voltage V_{Ci}, to which a series resistance R_i is connected, corresponding to the sum of the resistances of the switch and the capacitors. The load R_L is associated in parallel with a capacitor C_o, which

is initially discharged. Thus, the discharge occurs in two events. At first, the charge of capacitor C_i is divided between C_o and R_L. When the charge between the two capacitors is balanced, both start supplying R_L until they are completely discharged, as represented in Figure 25. At each stage, there is a different expression for the efficiency.

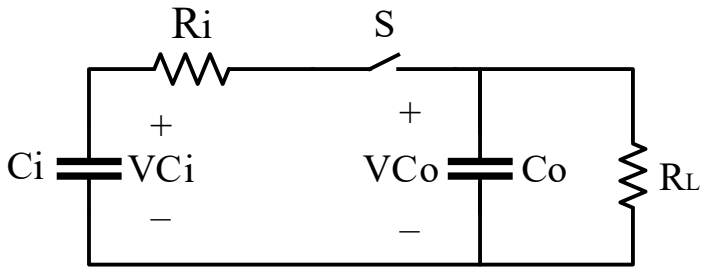

Figure 24. Circuit representing a capacitor discharging into a parallel RC circuit.

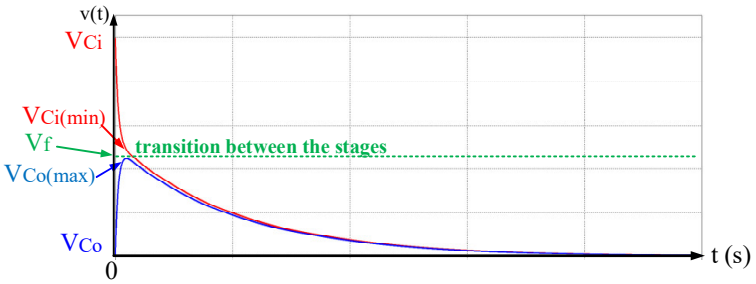

Figure 25. Waveforms representing a capacitor discharging into a parallel RC circuit.

In the first stage, the efficiency can be given by Equation (28).

$$\eta_1 = \left(\frac{V_{Co(\max)} + V_{Co}}{V_f + V_{Ci}} \right) \tag{28}$$

In the second stage, the efficiency can be estimated by Equation (29).

$$\eta_2 = \frac{R_L}{R_L + R_i} \tag{29}$$

In this analysis, the switching losses in the semiconductors must also be considered, although they have not been incorporated in the previous expressions. This is justified because adequately quantifying them depends on the intrinsic characteristics of each type of switch. In the case of MOSFETs, the increase in the switching frequency has direct impact on the switching losses as shown in Equation (4) [18,113]. On the other hand, when the switching frequency is increased, the voltage ripple is reduced. With a smaller voltage variation, the efficiency increases according to Expressions (23), (24), (26)–(28). Thus, it is up to the designer to carry out a detailed analysis regarding the best operation point for the circuit.

Analyzing the behavior of capacitors operating in no charge, partial charge, and full charge modes, it is reasonable to state that this methodology becomes valid for any converter topology because the operating principle of SC circuits is essentially based on the charge transfer from one element to another.

3.5. Regulation and Control

In this section, the most common control techniques applicable to SC converters are discussed since there is a significant voltage decrease when the load is connected to the output of such structures. The simplest way to increase the voltage gain in the case of

reducing the output voltage is to associate more cells in series. However, the higher the component count, the greater the series resistance in the circuit and, consequently, the lower the efficiency. A problem that can occur is the accuracy of the regulation capacity, as the connection of a second stage can excessively increase the output voltage.

Another solution that has less impact on efficiency is the achievement of voltage regulation using pulse width modulation (PWM) [124–126]. This technique is widely used to control the output voltage in the conventional buck, boost, and buck-boost converters. In SC circuits, this operation mode is divided into two stages per cycle. In the first stage, the capacitor is charged, and the duty cycle can assume values between $0 < D < 0.5$. In the second stage, the capacitor is connected to the load, and its discharge process begins. This situation is repeated during each cycle. It should be noted that when the duty cycle approaches zero, the voltage ripple increases and, consequently, the input current peaks increase [127].

Another strategy presented in the literature is the interleaved connection of cells [128]. However, this arrangement may or may not work with overlapping phases [128,129]. The main advantage lies in the fact that this method reduces the output voltage ripple, providing not only voltage regulation, but also an improvement in efficiency. However, as mentioned, it should be considered that a greater number of components causes an increase in losses. An advantage of this technique is the possibility of increasing the power levels considering that the current is shared among the interleaved cells.

The pulse frequency modulation (PFM) control technique is also well known in electronics. The advantage of this strategy lies in the simplicity of producing a variable frequency signal from monitoring the output voltage or output current. This signal increases the switching frequency according to the load current [130,131]. However, this technique does not guarantee reduced voltage ripple under heavy load conditions [132]. Another important point is that, when MOSFETs are used, increasing the switching frequency can increase switching losses according to (4).

A prominent control technique that takes advantage of the MOSFET transconductance is called quasi-switched capacitor (QSC). This strategy was formerly introduced in [133] as a new SC cell. Subsequent work used this concept in a somewhat obscure way while adopting the terms "QSC cell" and "QSC control". However, it can be regarded as technique for controlling the gate-source voltage in a MOSFET. When operating in the active region, that is, in the triode region, the drain current is proportional to the gate-source voltage [134]. If the MOSFET always operates in that region, the drain current can be controlled. The main difference in relation to the other techniques mentioned above is that the input current waveform does not change during the charge stage, while in other cases, there are short-term current peaks. In this way, this allows to reduce the current stresses on the switches and prevents the occurrence of conducted EMI. This control approach does not affect the converter efficiency, because, according to Expressions (23) and (24), the efficiency during the charge stage is dependent only on the difference between the voltage on the capacitor in charging process and the source voltage.

3.6. Comparison among SC Topologies

The existing SC topologies are very similar to each other in terms of constructive aspects, although they may differ with respect to the voltage gain, number of components, and stresses. The component count associated with the capacitors and switches required by a given basic cell is shown in Table 5 for a generic number of cells $N = 1, 2, 3, \ldots$. Besides, $F(N-1)$ is the $(N-1)$-th Fibonacci number, where $F(0) = F(1) = 1$. It is also worth mentioning that Table 5 summarizes the main characteristics of basic topologies used in the conception of SC dc-dc converters, which can assist the designer in choosing which configuration is more adequate for a given application.

Table 5. Comparison among SC topologies.

Parameters	SCVD	SPC	SPMC	Dickson	FC	Ladder *
Capacitors	N	N	$3N$	$2N$	N	$2N$
Switches	$4N$	$3N$	$3N$	$2N$	$3N$	$2N$
Maximum voltage on the capacitors for N-th cell	$2^{(N-1)}V_i$	V_i	V_i	NV_i	$F(N-1)V_i$	V_i
Maximum voltage on the switches for N-th cell	$2^{(N-1)}V_i$	NV_i	NV_i	V_i	$F(N-1)V_i$	V_i

* Boost mode.

It is observed that the voltage stresses on the capacitors increase as more cells are added to extend the conversion ratio in the SVCD and FC configurations. The maximum voltage stress on the active switches is constant and equal to the input voltage V_i in the Dickson and ladder converters, which makes them proper choices for applications involving high output voltages. The current stresses cannot be estimated in a such a simple manner because they do not depend only on the characteristics of the load connected to the converter, but also on the charge modes of the capacitors, which were discussed in Section 3.2.

SC circuits operating in full charge mode present high short-term current peaks, which occur when the capacitors are charged. The maximum value of the charging current must be taken into account carefully because it may damage the switch. Besides, the pulsating nature of the input current may lead to the increase of conducted electromagnetic emissions. Operation at high frequencies and/or the use of high capacitances to ensure the full charge or no charge condition are possible solutions that allow for mitigating such undesirable problems. The QSC is a control approach that can be used for this purpose as well as explained in Section 3.5. It allows obtaining a nearly continuous input current, thus causing the current stresses on the switches to be reduced as a consequence. Interleaved converters are also less susceptible to the undesirable effects caused by the voltage ripple on the capacitors as discussed in Section 3.5.

4. Applications

Conventional SC converters are widely used in practice, mainly at low power levels and when high power density is desired [35]. Such characteristics make them quite attractive for specific applications involving embedded electronic systems, biomedical equipment, energy harvesting, and general-purpose microelectronics. In this context, it is worth mentioning that some modern portable electronic devices have very low power consumption. For instance, smartphones consume approximately 1 W, while cardiac pacemakers consume 50 μW [135].

Several studies have discussed the relevance of using the available energy in the environment where a device or equipment is placed. Various forms of energy can be harvested and converted into electrical energy to power the aforementioned devices. Photovoltaic solar energy is a typical example [136–140], but other more unusual sources can be considered, such as pyroelectric [141–143] and blood sugar [144–146].

Regardless of the source, the applicability of SC converters in these cases has also drawn the attention of researchers in the case of other low-power applications [147–150]. Its use in the supply of sensors or very-low-power circuits is also possible, precisely in conditions in which space is limited [151–155].

Hybrid vehicles, which combine fossil fuels and energy storage devices such as supercapacitors and batteries, also constitute a favorable scenario for the use of SC converters [156,157]. In this case, the topologies can be employed to increase the voltage across the batteries and also to control the bidirectional power flow [47,158] aiming at the energy management and charge of the batteries [159–163]. Owing to the small size, one can even consider the integration of the whole set to the battery system itself as a consolidated solution.

SCVDs are often reported in the literature for applications rated at some milliwatts, which include electrically-erasable programmable read-only memories (EEPROMs), very large-scale integration (VLSI) systems VLSI [164,165], energy harvesting [152,154,166,167], and liquid crystal display (LCD) technology [168,169].

This technology can be used to supply electronic circuits such as operational amplifiers and analog-to-digital (A/D) converters, since this is the only type of SC configuration available in the form of commercial ICs. Table 6 shows some voltage doubler ICs available on the market, which are rated at low output currents and low input voltages.

SPC structures can be configured more simply with an array of encapsulated capacitors aiming at a wide range of options not only in series to increase the gain, but also in parallel to decrease the current ripple [170]. Existing applications are reported in a smaller number of publications owing to the control complexity. Among them, some circuits are proposed for energy harvesting in [150,151,153,171] and biomedical systems [172]. Since the SP topology is very versatile with respect to the voltage gain, the output voltage may remain constant even when there are large variations in the input voltage.

The Dickson converter was one of the first structures developed for practical applications involving memories [173–176]. The evolution of existing circuits is mainly concerned with the increase of energy density and efficiency. Some devices can even be integrated with the same memory chip [120,177].

The FC is similar to the SPC, but it requires a larger number of switches and capacitors. An emergency power supply for a computer system based on this structure was proposed in [178] as an emerging application, but LCD drivers can also be found in [179,180].

The ladder topology is also adequate for some specific applications, even though it is not very often used in DC-DC power conversion when compared with its remaining counterparts [181,182]. Among the topologies presented, this is the one with the highest efficiency and versatility. In experimental tests, the efficiency can be greater than 90% with low voltage ripple even at power levels on the order of 1 kW [183]. Thus, this is the only promising topology developed so far for high-power applications, while the others are only feasible at low power levels [170].

Table 6. Parameters of SCVD ICs.

IC	V_i (V)	I_o (mA)	η_{max} (%)
MAX660 [180]	1.8 to 5.5	100	88
LM2660 [184]	2.5 to 5.5	100	88
LM2685 [185]	2.85 to 6.5	50	80
MAX1680 [186]	2 to 5.5	5	90
MAX860 [187]	2 to 5.5	50	87
LT1054 [188]	3.5 to 15	100	NA
LM2665 [189]	2.5 to 5.5	40	90
LM2767 [190]	1.8 to 5.5	15	96
ADP3610 [191]	3 to 3.6	320	90
TCM828 [192]	1.5 to 5.5	25	95
GS7660 [193]	3 to 6	200	98

5. Conclusions

SC converters have drawn significant attention from academia and industry recently owing to their prominent characteristics associated with high energy density and low EMI levels in DC-DC, DC-AC, AC-DC, and AC-AC conversion. Considering that many hybrid SC topologies composed of capacitors, semiconductors, and inductors have been reported in the literature, this work has been specifically concerned with a general review of important concepts associated with "pure SC" DC-DC converters. The existing configurations were analyzed in detail, while a brief explanation on voltage multipliers was also included, considering that some structures are derived from such popular circuits used in low-power ac-dc power conversion.

It should be noted that pure SC converters employ only semiconductors and capacitors. Thus, it is reasonable to state that a successful design relies on the careful choice of such components, whose characteristics and impact on overall performance could be addressed in detail. Among controlled switches, MOSFETs are most used in practice owing to their ability to operate at high frequencies. In this context, the characteristics of required parts have an important role aimed at the increase of the converter efficiency. The capacitors, which are also a fundamental part of the circuit design, were analyzed in terms of the main characteristics of different types of technologies found on the market, such as film, ceramic, and electrolytic. It is worth mentioning that capacitors have direct impact on the converters size, while both the ESL and ESR limit the maximum operating frequency of the circuit.

During the design stage, it is very important to know inherent characteristics in operation modes of SC converters. Essentially, there are three distinct modes, each of which has a different impact on the circuit performance in terms of efficiency and regulation. From the previous knowledge of the intrinsic resistances of both capacitors and switches, it is possible to define a proper time constant aimed at achieving an adequate operating frequency for the converter. This aspect is also directly associated with the behavior of the output resistance of the circuit, which is inversely proportional to the conversion efficiency.

The control and voltage regulation techniques for SC DC-DC converters are still reported in a smaller number in the literature compared to those dedicated to the classic isolated and non-isolated DC-DC converters. Thus, this work was dedicated to the detailed analysis of the existing strategies for regulating the output voltage and obtaining reduced high-frequency ripple, since these aspects directly influence the efficiency significantly.

The classic control approach is based on PWM, but other techniques may also lead to good overall performance, e.g., PFM, especially because the duty cycle has little influence on the output voltage depending on the operation mode. The use of interleaved structures also provides good output voltage regulation and high efficiency due to the ripple minimization. Other more complex solutions, e.g., QSC, can also be used, with special concern to the reduction of the current peaks due to the operation of MOSFETs in the triode region.

Typical low-power applications of SC converters include general-purpose ICs, memories, and also energy harvesting for biomedical equipment owing to inherent high energy density. Considering the low efficiency typically achieved by SC structures in high-power applications, few publications are dedicated to the conception of power electronic converters based on capacitors and semiconductors only, i.e., without using inductors and transformers. However, more recently, the attention of many researchers has turned to the development of prominent structures for higher power levels. In this scenario, the efficiency analysis of SC converters considering the operation modes associated with the charging and discharging of capacitors is of major importance. It is also noteworthy that the ladder structure is an attractive solution for the development of power converters rated on the order of a few units of kilowatts.

Despite the apparently reduced complexity of the topologies, the design procedure must consider many variables. The characteristics of semiconductors and capacitors can drastically reduce the circuit efficiency if adequate components are not chosen. Another important aspect is the fact that the control methods are relatively complex, and do not act so responsively in the output voltage.

Even in the face of all the difficulties encountered in the development of these circuits, several modern applications highlight the great application potential of SC converters. Considering the constant search for miniaturization of electronic devices and the growing use of system on chip (SOC) type ICs, the topologies in question are among the main solutions that can be fully integrated into a single chip, since inductors do not allow that feature.

Author Contributions: Conceptualization, F.L.T. and E.R.R.; methodology, investigation, writing—original draft preparation, A.F.d.S. All authors have read and agreed to the published version of the manuscript.

Funding: This research was funded by the Federal University of Itajubá.

Data Availability Statement: Data available on request from the authors.

Acknowledgments: The authors acknowledge CAPES, CNPq, FAPEMIG, and INERGE for the overall support to this work.

Conflicts of Interest: The authors declare no conflict of interest.

References

1. Bose, B.K. Global energy scenario and impact of power electronics in 21st century. *IEEE Trans. Ind. Electron.* **2013**, *60*, 2638–2651. [CrossRef]
2. Baliga, B.J. Trends in power semiconductor devices. *IEEE Trans. Electron. Devices* **1996**, *43*, 1717–1731. [CrossRef]
3. Bose, B.K. Evaluation of modern power semiconductor devices and future trends of converters. *IEEE Trans. Ind. Appl.* **1992**, *28*, 403–413. [CrossRef]
4. Biela, J.; Schweizer, M.; Waffler, S.; Kolar, J.W. SiC versus Si—evaluation of potentials for performance improvement of inverter and DC–DC converter systems by SiC power semiconductors. *IEEE Trans. Ind. Electron.* **2011**, *58*, 2872–2882. [CrossRef]
5. Zhan, A.; Dang, G.T.; Ren, F.; Cho, H.; Lee, K.-P.; Pearton, S.J.; Chyi, J.-I.; Nee, T.-Y.; Chuo, C.-C. Comparison of GaN pin and Schottky rectifier performance. *IEEE Trans. Electron Devices* **2001**, *48*, 407–411. [CrossRef]
6. Chowdhury, S.; Stum, Z.; Li, Z.D.; Ueno, K.; Chow, T.P. Comparison of 600V Si, SiC and GaN power devices. *Mater. Sci. Forum* **2014**, *778–780*, 971–974. [CrossRef]
7. González, A.; Goikolea, E.; Barrena, J.A.; Mysyk, R. Review on supercapacitors: Technologies and materials. *Renew. Sustain. Energy Rev.* **2016**, *58*, 1189–1206. [CrossRef]
8. Zubieta, L.; Bonert, R. Characterization of double-layer capacitors (DLCs) for power electronics applications. In Proceedings of the Conference Record of 1998 IEEE Industry Applications Conference. Thirty-Third IAS Annual Meeting (Cat. No.98CH36242), Saint Louis, MO, USA, 12–15 October 1998; Volume 2, pp. 1149–1154.
9. Shokrollahi, H.; Janghorban, K. Soft magnetic composite materials (SMCs). *J. Mater. Process. Technol.* **2007**, *189*, 1–12. [CrossRef]
10. Kunz, W.; Grätzer, D. Amorphous alloys for switched-mode power supplies. *J. Magn. Magn. Mater.* **1980**, *19*, 183–184. [CrossRef]
11. Li, Z.; Yao, K.; Li, D.; Ni, X.; Lu, Z. Core loss analysis of Finemet type nanocrystalline alloy ribbon with different thickness. *Prog. Nat. Sci. Mater. Int.* **2017**, *27*, 588–592. [CrossRef]
12. Texas Instruments. LM2750 Low-Noise Switched-Capacitor Boost Regulator. Available online: http://www.ti.com/lit/ds/symlink/lm2750.pdf (accessed on 1 March 2021).
13. ON Semiconductor. NCP 1719 Switched Capacitor Voltage Inverter. Available online: https://www.onsemi.com/pub/Collateral/NCP1729-D.PDF (accessed on 1 March 2021).
14. Tan, S.-C.; Nur, M.; Kiratipongvoot, S.; Bronstein, S.; Lai, Y.-M.; Tse, C.; Ioinovici, A. Switched-capacitor converter configuration with low EMI emission obtained by interleaving and its large-signal modeling. In Proceedings of the 2009 IEEE International Symposium on Circuits and Systems, Taipei, Taiwan, 24–27 May 2009; pp. 1081–1084.
15. Ioinovici, A. Switched-capacitor power electronics circuits. *IEEE Circ. Syst. Mag.* **2001**, *1*, 37–42. [CrossRef]
16. Tsai, K.; Qi, F.; Davidson, E.; Xu, L. Common mode EMI noise characterization and improvement for GaN switched-capacitor converter. In Proceedings of the IEEE Energy Conversion Congress and Exposition, Denver, CO, USA, 15–19 September 2013; pp. 4159–4165.
17. Zhu, G.; Ioinovici, A. Steady-state characteristics of switched-capacitor electronic converters. *J. Circ. Syst. Comput.* **1997**, *7*, 69–91. [CrossRef]
18. Guangyong, Z.; Ioinovici, A. Switched-capacitor power supplies: DC voltage ratio, efficiency, ripple, regulation. In Proceedings of the IEEE International Symposium on Circuits and Systems (ISCAS), Atlanta, GA, USA, 15 May 1996; pp. 553–556.
19. Zhu, G.; Wei, H.; Batarseh, I.; Ioinovici, A. A new switched-capacitor dc-dc converter with improved line and load regulations. In Proceedings of the IEEE International Symposium on Circuits and Systems (ISCAS), Orlando, FL, USA, 30 May–2 June 1999; pp. 234–237.
20. Das, R.; Seo, G.; Le, H. Analysis of dual-inductor hybrid converters for extreme conversion ratios. *IEEE J. Emerg. Sel. Top. Power Electron.* **2020**, 1–13. [CrossRef]
21. Assem, P.; Liu, W.; Lei, Y.; Hanumolu, P.K.; Pilawa-Podgurski, R.C.N. Hybrid Dickson switched-capacitor converter with wide conversion ratio in 65-nm CMOS. *IEEE J. Solid State Circ.* **2020**, *55*, 2513–2528. [CrossRef]
22. Oualkadi, A.E.; Cordeau, D.; Paillot, J. High-Q CMOS LC pseudo switched-capacitor bandpass filter with center frequency tuning. In Proceedings of the IEEE International Symposium on Circuits and Systems, Kos, Greece, 21–24 May 2006; p. 3909.
23. Ye, Z.; Lei, Y.; Pilawa-Podgurski, R.C.N. The cascaded resonant converter: A hybrid switched-capacitor topology with high power density and efficiency. *IEEE Trans. Power Electron.* **2020**, *35*, 4946–4958. [CrossRef]

24. Ura, K. Contrast mechanism of negatively charged insulators in scanning electron microscope. *Microscopy* **1998**, *47*, 143–147. [CrossRef]
25. Iqbal, S.; Singh, G.K.; Besar, R. A dual-mode input voltage modulation control scheme for voltage multiplier based X-ray power supply. *IEEE Trans. Power Electron.* **2008**, *23*, 1003–1008. [CrossRef]
26. Sun, J.; Ding, X.; Nakaoka, M.; Takano, H. Series resonant ZCS–PFM DC–DC converter with multistage rectified voltage multiplier and dual-mode PFM control scheme for medical-use high-voltage X-ray power generator. *IEE Proc. Electr. Power Appl.* **2000**, *147*, 527–534. [CrossRef]
27. Ahmed, F.U.; Chowdhury, M.H. An asynchronous reconfigurable switched capacitor voltage regulator. In Proceedings of the IEEE 61st International Midwest Symposium on Circuits and Systems (MWSCAS), Windsor, ON, Canada, 5–8 August 2018; pp. 1110–1113.
28. Chen, C.; Liu, X. A high-efficiency switched capacitor converter for always-on block. In Proceedings of the 14th IEEE International Conference on Solid State and Integrated Circuit Technology (ICSICT), Qingdao, China, 31 October–3 November 2018; pp. 1–3.
29. Lei, H.; Hao, R.; You, X.; Li, F.; Zhou, M. Nonisolated high step-up soft-switching DC-DC converter integrating Dickson switched-capacitor techniques. In Proceedings of the IEEE Energy Conversion Congress and Exposition (ECCE), Portland, OR, USA, 23–27 September 2018; pp. 1247–1252.
30. Jiang, J.; Liu, X.; Ki, W.; Mok, P.K.T.; Lu, Y. A multiphase switched-capacitor converter for fully integrated AMLED microdisplay system. *IEEE Trans. Power Electron.* **2020**, *35*, 6001–6011. [CrossRef]
31. Shah, N.; Lajevardi, P.; Wojciechowski, K.; Lang, C.; Murmann, B. An energy harvester using image sensor pixels with cold start and over 96% MPPT efficiency. *IEEE Solid State Circ. Lett.* **2019**, *2*, 207–210. [CrossRef]
32. Chiou, C.W.; Sun, Y.; Lee, C.; Liou, J. Low-complexity unidirectional systolic Dickson basis multiplier for lightweight cryptosystems. *Electron. Lett.* **2019**, *55*, 28–30. [CrossRef]
33. Gunnam, L.C.; Lai, Y.; Sung, G. Differential Dickson voltage multiplier with matching network for radio frequency harvester. In Proceedings of the IEEE International Conference on Consumer Electronics, Taiwan (ICCE-TW), Taipei, Taiwan, 12–14 June 2017; pp. 417–418.
34. Dela Cruz, S.; delos Reyes, M.G.; Alvarez, A.; de Leon, M.T.; Roque, C.R. Design and implementation of passive RF-DC converters for RF power harvesting systems. In Proceedings of the TENCON, 2010 IEEE Region 10 Conference, Fukoka, Japan, 21–24 November 2010; pp. 1503–1508.
35. Forouzesh, M.; Siwakoti, Y.P.; Gorji, S.A.; Blaabjerg, F.; Lehman, B. Step-up DC–DC converters: A comprehensive review of voltage-boosting techniques, topologies, and applications. *IEEE Trans. Power Electron.* **2017**, *32*, 9143–9178. [CrossRef]
36. Arfin, S.; Mamun, A.A.; Chowdhury, T.; Sarowar, G. Zeta based hybrid DC-DC converter using switched inductor and switched capacitor combined structure for high gain applications. In Proceedings of the IEEE International Conference on Power, Electrical, and Electronics and Industrial Applications (PEEIACON), Dhaka, Bangladesh, 29 November–1 December 2019; pp. 1–4.
37. Axelrod, B.; Berkovich, Y.; Ioinovici, A. Switched-capacitor (SC)/switched inductor (SL) structures for getting hybrid step-down Cuk/Sepic/Zeta converters. In Proceedings of the IEEE International Symposium on Circuits and Systems, Kos, Greece, 21–24 May 2006; p. 4.
38. Banaei, M.R.; Kazemi, F.M. A modified selective harmonic elimination switching strategy for Hybrid Flying Capacitor Multicell converter. In Proceedings of the 7th International Conference on Electrical and Electronics Engineering (ELECO), Bursa, Turkey, 1–4 December 2011; pp. I-278–I-282.
39. Bhaskar, M.; Ganesan, R.G.; Narayanan, K. Interleaved hybrid boost converter with switched capacitor technique. In Proceedings of the IEEE Innovative Smart Grid Technologies, Asia (ISGT Asia), Chengdu, China, 21–24 May 2019; pp. 3890–3895.
40. Chen, M.; Hu, J.; Li, K.; Ioinovici, A. A new switched-capacitor based hybrid converter with large step-up DC gain and low voltage on its semiconductors. In Proceedings of the IEEE International Symposium on Circuits and Systems (ISCAS), Montreal, QC, Canada, 22–25 May 2016; pp. 1190–1193.
41. Chen, M.; Li, K.; Hu, J.; Ioinovici, A. Hybrid switched-capacitor quadratic boost converters with very high DC gain and low voltage stress on their semiconductor devices. In Proceedings of the IEEE Energy Conversion Congress and Exposition (ECCE), Milwaukee, WI, USA, 18–22 September 2016; pp. 1–8.
42. Dantas, M.; Oliveira, F.; Albuquerque, L.; Freitas, I.; Andersen, R. A hybrid bidirectional push-pull DC-DC converter with a ladder switched-capacitor cell. In Proceedings of the IEEE 15th Brazilian Power Electronics Conference and 5th IEEE Southern Power Electronics Conference (COBEP/SPEC), Santos, Brazil, 1–4 December 2019; pp. 1–6.
43. Eate, V.K.; Veerachary, M. Analysis of two-input Switched Inductor-Capacitor Hybrid Buck-SEPIC DC-DC converter. In Proceedings of the IEEE Transportation Electrification Conference (ITEC-India), Pune, India, 13–15 December 2017; pp. 1–6.
44. Hulea, D.; Muntean, N.; Gireada, M.; Cornea, O. A bidirectional hybrid switched-capacitor DC-DC converter with a high voltage gain. In Proceedings of the International Aegean Conference on Electrical Machines and Power Electronics (ACEMP) & 2019 International Conference on Optimization of Electrical and Electronic Equipment (OPTIM), Istanbul, Turkey, 27–29 August 2019; pp. 289–296.
45. Hulea, D.; Muntean, N.; Gireada, M.; Cornea, O.; Serban, E. Bidirectional hybrid switched-inductor switched-capacitor converter topology with high voltage gain. In Proceedings of the 21st European Conference on Power Electronics and Applications (EPE 2019 ECCE Europe), Genova, Italy, 3–5 September 2019; pp. 1–10.

46. Janabi, A.; Wang, B. Switched-capacitor voltage boost converter for electric and hybrid electric vehicle drives. *IEEE Transact. Power Electron.* **2020**, *35*, 5615–5624. [CrossRef]
47. Li, S.; Zheng, Y.; Wu, B.; Smedley, K.M. A family of resonant two-switch boosting switched-capacitor converter with ZVS operation and a wide line regulation range. *IEEE Transact. Power Electron.* **2018**, *33*, 448–459. [CrossRef]
48. Kumar, P.; Veerachary, M. Hybrid switched inductor/switched capacitor based quasi-Z-source DC-DC boost converter. In Proceedings of the 2nd IEEE International Conference on Power Electronics, Intelligent Control and Energy Systems (ICPEICES), Delhi, India, 22–24 October 2018; pp. 617–622.
49. Leandro, G.M.; Barbi, I. DC-DC hybrid switched-capacitor LLC resonant converter: All switches with VDS=Vin/2. In Proceedings of the IEEE PES Innovative Smart Grid Technologies Conference–Latin America (ISGT Latin America), Gramado, Brazil, 15–18 September 2019; pp. 1–6.
50. Lei, Y.; Liu, W.; Pilawa-Podgurski, R.C.N. An analytical method to evaluate flying capacitor multilevel converters and hybrid switched-capacitor converters for large voltage conversion ratios. In Proceedings of the IEEE 16th Workshop on Control and Modeling for Power Electronics (COMPEL), Vancouver, BC, Canada, 12–15 July 2015; pp. 1–7.
51. Lei, Y.; Liu, W.; Pilawa-Podgurski, R.C.N. An analytical method to evaluate and design hybrid switched-capacitor and multilevel converters. *IEEE Trans. Power Electron.* **2018**, *33*, 2227–2240. [CrossRef]
52. Lei, Y.; Ye, Z.; Pilawa-Podgurski, R.C.N. A GaN-based 97% efficient hybrid switched-capacitor converter with lossless regulation capability. In Proceedings of the IEEE Energy Conversion Congress and Exposition (ECCE), Montreal, QC, Canada, 20–24 September 2015; pp. 4264–4270.
53. Li, G.; Zhiming, C.; Jian, L. Design of a hybrid monolithic integrated switched capacitor DC-DC step-up converter. In Proceedings of the IPEMC 2000. Third International Power Electronics and Motion Control Conference (IEEE Cat. No.00EX435), Beijing, China, 15–18 August 2000; pp. 263–266.
54. Pelan, O.; Muntean, N.; Cornea, O. Comparative evaluation of buck and switched-capacitor hybrid buck DC-DC converters. In Proceedings of the International Symposium on Power Electronics Power Electronics, Electrical Drives, Automation and Motion, Sorrento, Italy, 20–22 June 2012; pp. 1330–1335.
55. Sadigh, A.K.; Dargahi, V.; Corzine, K.A. Reduction of switches and flying capacitors in a hybrid topology of the stacked multicell converters. In Proceedings of the IECON 2019, 45th Annual Conference of the IEEE Industrial Electronics Society, Lisbon, Portugal, 14–17 October 2019; pp. 4977–4982.
56. Sarath, R.; Kanakasabapathy, P. Switched-capacitor/switched-inductor Ćuk-derived hybrid converter for nanogrid applications. In Proceedings of the International Conference on Computation of Power, Energy, Information and Communication (ICCPEIC), Melmaruvathur, India, 22–23 April 2015; pp. 430–435.
57. Soares, M.V.; Lambert, G.; Novaes, Y.R. Hybrid switched capacitor DC-DC converter based on MMC. In Proceedings of the IEEE 15th Brazilian Power Electronics Conference and 5th IEEE Southern Power Electronics Conference (COBEP/SPEC), Santos, Brazil, 1–4 December 2019; pp. 1–6.
58. Stewart, J.; Richards, J.; Delhotal, J.; Neely, J.; Flicker, J.; Brocato, R.; Rashkin, L. Design and evaluation of hybrid switched capacitor converters for high voltage, high power density applications. In Proceedings of the IEEE Applied Power Electronics Conference and Exposition (APEC), San Antonio, TX, USA, 4–8 March 2018; pp. 105–112.
59. Tewari, N.; Sreedevi, V.T. Switched inductor-switched capacitor based high gain hybrid dc-dc converter. In Proceedings of the 8th IEEE India International Conference on Power Electronics (IICPE), Jaipur, India, 13–15 December 2018; pp. 1–6.
60. Vecchia, M.D.; Lazzarin, T.B. A hybrid switched capacitor DC-DC buck converter. In Proceedings of the IEEE 13th Brazilian Power Electronics Conference and 1st Southern Power Electronics Conference (COBEP/SPEC), Fortaleza, Brazil, 29 November–2 December 2015; pp. 1–6.
61. Vecchia, M.D.; Lazzarin, T.B. Hybrid DC-DC buck converter with active switched capacitor cell and low voltage gain. In Proceedings of the IEEE Energy Conversion Congress and Exposition (ECCE), Milwaukee, WI, USA, 18–22 September 2016; pp. 1–6.
62. Veerachary, M.; Reddy, T.N. Voltage-mode control of hybrid switched capacitor converters. In Proceedings of the IECON 2006, 32nd Annual Conference on IEEE Industrial Electronics, Paris, France, 6–10 November 2006; pp. 2450–2453.
63. Veerachary, M.; Reddy, T.N. Design and control of hybrid switched capacitor DC-DC converter with different operating conditions. In Proceedings of the International Conference on Advances in Computing, Control, and Telecommunication Technologies, Bangalore, India, 28–29 December 2009; pp. 559–563.
64. Veerachary, M.; Sudhakar, S.B. Peak-current mode control of hybrid switched capacitor converter. In Proceedings of the International Conference on Power Electronic, Drives and Energy Systems, New Delhi, India, 12–15 December 2006; pp. 1–6.
65. Xiong, S.; Tan, S.; Wong, S. Analysis of a high-voltage-gain hybrid switched-capacitor buck converter. In Proceedings of the IEEE International Symposium of Circuits and Systems (ISCAS), Rio de Janeiro, Brazil, 15–18 May 2011; pp. 1616–1619.
66. Greinacher, H. The ionometer and its application to the measurement of radium and röntgen rays. *Phys. Z.* **1914**, *15*, 410–415.
67. Kind, D.; Feser, K. *High Voltage Test Techniques*; Elsevier: Amsterdam, The Netherlands, 2001.
68. Hwang, F.; Shen, Y.; Jayaram, S.H. Low-ripple compact high-voltage DC power supply. *IEEE Trans. Ind. Appl.* **2006**, *42*, 1139–1145. [CrossRef]
69. Fukuyama, T.; Sugihara, K. Study on operating principle of Cockcroft-Walton circuit to produce plasmas using high-voltage discharge. *Plasma Fusion Res.* **2016**, *11*, 2401008. [CrossRef]

70. Midya, P. Efficiency analysis of switched capacitor doubler. In Proceedings of the 39th Midwest Symposium on Circuits and Systems, Ames, IA, USA, 21–21 August 1996; pp. 1019–1022.
71. Cataldo, G.D.; Palumbo, G. Double and triple charge pump for power IC: Dynamic models which take parasitic effects into account. In *IEEE Transactions on Circuits and Systems I: Fundamental Theory and Applications*; IEEE: Piscataway, NJ, USA, 1993; Volume 40, pp. 92–101.
72. Cockcroft, J.D.; Walton, E.T. Experiments with high velocity positive ions. (I) Further developments in the method of obtaining high velocity positive ions. *Proc. Math. Phys. Eng. Sci.* **1932**, *136*, 619–630.
73. Müller, L.; Kimball, J.W. Dual-input high gain DC-DC converter based on the Cockcroft-Walton multiplier. In Proceedings of the IEEE Energy Conversion Congress and Exposition (ECCE), Pittsburgh, PA, USA, 14–18 September 2014; pp. 5360–5367.
74. Müller, L.; Kimball, J.W. High gain DC–DC converter based on the Cockcroft–Walton multiplier. *IEEE Trans. Power Electron.* **2016**, *31*, 6405–6415. [CrossRef]
75. Young, C.; Chen, M. A novel single-phase ac to high voltage dc converter based on Cockcroft-Walton cascade rectifier. In Proceedings of the International Conference on Power Electronics and Drive Systems (PEDS), Taipei, Taiwan, 2–5 November 2009; pp. 822–826.
76. Young, C.; Chun-Cho, K.; Chen, M.; Chao-Cheng, W. A Cockcroft-Walton voltage multiplier with PFC using ZC-ZVT auxiliary circuit. In Proceedings of the IECON 2011, 37th Annual Conference of the IEEE Industrial Electronics Society, Melbourne, VIC, Australia, 7–10 November 2011; pp. 1000–1005.
77. Young, C.; Chen, M.; Hong-Lin, C.; Jen-Yi, C.; Chun-Cho, K. Transformerless single-stage high step-up AC-DC converter based on symmetrical Cockcroft-Walton voltage multiplier with PFC. In Proceedings of the IEEE Ninth International Conference on Power Electronics and Drive Systems, Singapore, 5–8 December 2011; pp. 191–196.
78. Kobougias, I.C.; Tatakis, E.C. Optimal design of a half-wave Cockroft-Walton voltage multiplier with different capacitances per stage. *IEEE Transact. Power Electron.* **2010**, *25*, 2460–2468. [CrossRef]
79. Brugler, J.S. Theoretical performance of voltage multiplier circuits. *IEEE J. Solid State Circ.* **1971**, *6*, 132–135. [CrossRef]
80. Tanzawa, T. *On-Chip High-Coltage Generator Design*; Springer: Berlin/Heidelberg, Germany, 2013.
81. Falkner, A. Generalised cockcroft-walton voltage multipliers. *Electron. Lett.* **1973**, *9*, 585–586. [CrossRef]
82. Dickson, J.F. On-chip high-voltage generation in MNOS integrated circuits using an improved voltage multiplier technique. *IEEE J. Solid State Circ.* **1976**, *11*, 374–378. [CrossRef]
83. Alzahrani, A.; Shamsi, P.; Ferdowsi, M. Analysis and design of bipolar Dickson DC-DC converter. In Proceedings of the IEEE Power and Energy Conference at Illinois (PECI), Champaign, IL, USA, 23–24 February 2017; pp. 1–6.
84. Tanzawa, T.; Tanaka, T. A dynamic analysis of the Dickson charge pump circuit. *IEEE J. Solid State Circ.* **1997**, *32*, 1231–1240. [CrossRef]
85. Tanzawa, T. A switch-resistance-aware Dickson charge pump model for optimizing clock frequency. *IEEE Trans. Circ. Syst. II Express Briefs* **2011**, *58*, 336–340. [CrossRef]
86. Makowski, M.S.; Maksimovic, D. Performance limits of switched-capacitor DC-DC converters. In Proceedings of the PESC 1995, Power Electronics Specialist Conference, Atlanta, GA, USA, 18–22 June 1995; pp. 1215–1221.
87. Makowski, M.S. Realizability conditions and bounds on synthesis of switched-capacitor DC-DC voltage multiplier circuits. *IEEE Trans. Circ. Syst. I Regul. Pap.* **1997**, *44*, 684–691. [CrossRef]
88. Meynard, T.A.; Foch, H. Multi-level conversion: High voltage choppers and voltage-source inverters. In Proceedings of the PESC 19992 Record, 23rd Annual IEEE Power Electronics Specialists Conference, Toledo, Spain, 29 June–3 July 1992; pp. 397–403.
89. Meynard, T.A.; Foch, H.; Thomas, P.; Courault, J.; Jakob, R.; Nahrstaedt, M. Multicell converters: Basic concepts and industry applications. *IEEE Trans. Ind. Electron.* **2002**, *49*, 955–964. [CrossRef]
90. Lazzarin, T.B.; Andersen, R.L.; Martins, G.B.; Barbi, I. A 600-W switched-capacitor AC–AC converter for 220 V/110 V and 110 V/220 V applications. *IEEE Trans. Power Electron.* **2012**, *27*, 4821–4826. [CrossRef]
91. Östling, M.; Ghandi, R.; Zetterling, C. SiC power devices–Present status, applications and future perspective. In Proceedings of the IEEE 23rd International Symposium on Power Semiconductor Devices and ICs, San Diego, CA, USA, 23–26 May 2011; pp. 10–15.
92. Tanabe, H.; Kojima, T.; Imakiire, A.; Fuji, K.; Kozako, M.; Hikita, M. Comparison performance of Si-IGBT and SiC-MOSFET used for high efficiency inverter of contactless power transfer system. In Proceedings of the IEEE 11th International Conference on Power Electronics and Drive Systems, Sydney, NSW, Australia, 9–12 June 2015; pp. 707–710.
93. Wang, G.; Wang, F.; Magai, G.; Lei, Y.; Huang, A.; Das, M. Performance comparison of 1200V 100A SiC MOSFET and 1200V 100A silicon IGBT. In Proceedings of the IEEE Energy Conversion Congress and Exposition, Denver, CO, USA, 15–19 September 2013; pp. 3230–3234.
94. Baliga, B.J. *Fundamentals of Power Semiconductor Devices*; Springer: Berlin/Heidelberg, Germany, 2010.
95. Rashid, M.H. *Power Electronics Handbook: Devices, Circuits and Applications*; Elsevier: Amsterdam, The Netherlands, 2010.
96. Ahmed, A. *Power Electronics for Technology*; Pearson: New York, NY, USA, 1998.
97. Ye, Y.; Chen, S.; Yi, Y. Switched-capacitor and coupled-inductor based high step-up converter with improved voltage gain. *IEEE J. Emerg. Sel. Top. Power Electron.* **2021**, *9*, 754–764. [CrossRef]
98. Harada, K.; Katsuki, A.; Fujiwara, M. Use of ESR for deterioration diagnosis of electrolytic capacitor. *IEEE Trans. Power Electron.* **1993**, *8*, 355–361. [CrossRef]

99. Ahmad, M. A simple scheme for loss angle measurement of a capacitor. *IEEE Trans. Energy Convers.* **2004**, *19*, 228–229. [CrossRef]
100. Ramm, G.; Moser, H. From the calculable AC resistor to capacitor dissipation factor determination on the basis of time constants. *IEEE Trans. Instrum. Meas.* **2001**, *50*, 286–289. [CrossRef]
101. Fiore, R. ESR Losses in Ceramic Capacitors. Available online: www.atceramics.com (accessed on 1 March 2021).
102. Roy, T.; Smith, L.; Prymak, J. ESR and ESL of ceramic capacitor applied to decoupling applications. In Proceedings of the IEEE 7th Topical Meeting on Electrical Performance of Electronic Packaging (Cat. No.98TH8370), West Point, NY, USA, 26–28 October 1998; pp. 213–216.
103. Gebbia, M. Low ESR capacitors: Fact or fiction? *ECN Luty* **2001**, *200*.
104. Anderson, R. Select the right plastic film capacitor for your power electronic applications. In Proceedings of the IAS 1996, Conference Record of the 1996 IEEE Industry Applications Conference Thirty-First IAS Annual Meeting, San Diego, CA, USA, 6–10 October 1996; pp. 1327–1330.
105. Tortai, J.; Denat, A.; Bonifaci, N. Self-healing of capacitors with metallized film technology: Experimental observations and theoretical model. *J. Electrost.* **2001**, *53*, 159–169. [CrossRef]
106. Borghetti, A.; Nucci, C.A.; Pasini, G.; Pirani, S.; Rinaldi, M. Tests on self-healing metallized polypropylene capacitors for power applications. *IEEE Trans. Power Deliv.* **1995**, *10*, 556–561. [CrossRef]
107. Chen, Y.; Li, H.; Lin, F.; Lv, F.; Zhang, M.; Li, Z.; Liu, D. Study on self-healing and lifetime characteristics of metallized-film capacitor under high electric field. *IEEE Trans. Plasma Sci.* **2012**, *40*, 2014–2019. [CrossRef]
108. Makdessi, M.; Sari, A.; Venet, P. Metallized polymer film capacitors ageing law based on capacitance degradation. *Microelectron. Reliab.* **2014**, *54*, 1823–1827. [CrossRef]
109. Pan, M.; Randall, C.A. A brief introduction to ceramic capacitors. *IEEE Electr. Insul. Mag.* **2010**, *26*, 44–50. [CrossRef]
110. Young, A.L.; Hilmas, G.E.; Zhang, S.C.; Schwartz, R.W. Mechanical vs. electrical failure mechanisms in high voltage, high energy density multilayer ceramic capacitors. *J. Mater. Sci.* **2007**, *42*, 5613–5619. [CrossRef]
111. Oota, I.; Hara, N.; Ueno, F. A general method for deriving output resistances of serial fixed type switched-capacitor power supplies. In Proceedings of the IEEE International Symposium on Circuits and Systems (ISCAS), Geneva, Switzerland, 28–31 May 2000; pp. 503–506.
112. Seeman, M.D. *A Design Methodology for Switched-Capacitor DC-DC Converters*; University of California: Berkeley, CA, USA, 2009.
113. Seeman, M.D.; Sanders, S.R. Analysis and optimization of switched-capacitor DC–DC converters. *IEEE Trans. Power Electron.* **2008**, *23*, 841–851. [CrossRef]
114. Ben-Yaakov, S. Behavioral average modeling and equivalent circuit simulation of switched capacitors converters. *IEEE Trans. Power Electron.* **2012**, *27*, 632–636. [CrossRef]
115. Ben-Yaakov, S. On the influence of switch resistances on switched-capacitor converter losses. *IEEE Trans. Ind. Electron.* **2012**, *59*, 638–640. [CrossRef]
116. Wei-Chung, W.; Bass, R.M. Analysis of charge pumps using charge balance. In Proceedings of the IEEE 31st Annual Power Electronics Specialists Conference, Galway, Ireland, 23–23 June 2000; pp. 1491–1496.
117. Lazzarin, T.B.; Andersen, R.L.; Barbi, I. A switched-capacitor three-phase AC–AC converter. *IEEE Trans. Ind. Electron.* **2015**, *62*, 735–745. [CrossRef]
118. Ben-Yaakov, S.; Evzelman, M. Generic and unified model of Switched Capacitor Converters. In Proceedings of the IEEE Energy Conversion Congress and Exposition, San Jose, CA, USA, 20–24 September 2009; pp. 3501–3508.
119. Kimball, J.W.; Krein, P.T.; Cahill, K.R. Modeling of capacitor impedance in switching converters. *IEEE Power Electron. Lett.* **2005**, *3*, 136–140. [CrossRef]
120. Favrat, P.; Deval, P.; Declercq, M.J. A high-efficiency CMOS voltage doubler. *IEEE J. Solid State Circ.* **1998**, *33*, 410–416. [CrossRef]
121. Chang, Y.-H. Design and analysis of power-CMOS-gate-based switched-capacitor boost DC-AC inverter. *IEEE Trans. Circ. Syst. I Regul. Pap.* **2004**, *51*, 1998–2016. [CrossRef]
122. Henry, J.M.; Kimball, J.W. Practical performance analysis of complex switched-capacitor converters. *IEEE Trans. Power Electron.* **2011**, *26*, 127–136. [CrossRef]
123. Cheung, C.-K.; Tan, S.-C.; Chi, K.T.; Ioinovici, A. On energy efficiency of switched-capacitor converters. *IEEE Trans. Power Electron.* **2012**, *28*, 862–876. [CrossRef]
124. On-Cheong, M.; Yue-Chung, W.; Ioinovici, A. Step-up DC power supply based on a switched-capacitor circuit. *IEEE Trans. Ind. Electron.* **1995**, *42*, 90–97. [CrossRef]
125. Cheong, S.V.; Chung, H.; Ioinovici, A. Inductorless DC-to-DC converter with high power density. *IEEE Trans. Ind. Electron.* **1994**, *41*, 208–215. [CrossRef]
126. Cheong, S.V.; Chung, S.H.; Ioinovici, A. Development of power electronics converters based on switched-capacitor circuits. In Proceedings of the 1992 IEEE International Symposium on Circuits and Systems, San Diego, CA, USA, 10–13 May 1992; Volume 4, pp. 1907–1910.
127. Suetsugu, T. Novel PWM control method of switched capacitor DC-DC converter. In Proceedings of the ISCAS 1998 IEEE International Symposium on Circuits and Systems (Cat. No. 98CH36187), Monterey, CA, USA, 31 May–3 June 1998; pp. 454–457.
128. Tan, S.; Kiratipongvoot, S.; Bronstein, S.; Ioinovici, A.; Lai, Y.M.; Tse, C.K. Interleaved switched-capacitor converters with adaptive control. In Proceedings of the IEEE Energy Conversion Congress and Exposition, Atlanta, GA, USA, 12–16 September 2010; pp. 2725–2732.

129. Huang, M.; Fan, P.; Chen, K. Low-ripple and dual-phase charge pump circuit regulated by switched-capacitor-based bandgap reference. *IEEE Trans. Power Electron.* **2009**, *24*, 1161–1172. [CrossRef]
130. Kilani, D.; Alhawari, M.; Mohammad, B.; Saleh, H.; Ismail, M. An efficient switched-capacitor DC-DC buck converter for self-powered wearable electronics. *IEEE Trans. Circ. Syst. I Regul. Pap.* **2016**, *63*, 1557–1566. [CrossRef]
131. Veerabathini, A.; Furth, P.M. High-efficiency switched-capacitor DC-DC converter with three decades of load current range using adaptively-biased PFM. *J. Low Power Electron. Appl.* **2020**, *10*, 5. [CrossRef]
132. Bahry, M.K.; El-Nozahi, M.; Hegazi, E. A PFM-regulated switched-capacitor DC-DC converter with enhanced-ripples technique. In Proceedings of the 29th International Conference on Microelectronics (ICM), Beirut, Lebanon, 10–13 December 2017; pp. 1–4.
133. Chung, H.; Ioinovici, A. Switched-capacitor-based DC-to-DC converter with improved input current waveform. In Proceedings of the IEEE International Symposium on Circuits and Systems. Circuits and Systems Connecting the World. ISCAS 96, Atlanta, GA, USA, 15 May 1996; pp. 541–544.
134. Chung, H. Design and analysis of quasi-switched-capacitor step-up dc/dc converters. In Proceedings of the ISCAS'98, Proceedings of the IEEE International Symposium on Circuits and Systems (Cat. No. 98CH36187), Monterey, CA, USA, 31 May–3 June 1998; pp. 438–441.
135. Vullers, R.; van Schaijk, R.; Doms, I.; Van Hoof, C.; Mertens, R. Micropower energy harvesting. *Solid State Electron.* **2009**, *53*, 684–693. [CrossRef]
136. Raghunathan, V.; Kansal, A.; Hsu, J.; Friedman, J.; Srivastava, M. Design considerations for solar energy harvesting wireless embedded systems. In Proceedings of the IPSN 2005. Fourth International Symposium on Information Processing in Sensor Networks, Boise, ID, USA, 15 April 2005; pp. 457–462.
137. Guilar, N.J.; Kleeburg, T.J.; Chen, A.; Yankelevich, D.R.; Amirtharajah, R. Integrated solar energy harvesting and storage. *IEEE Trans. Very Large Scale Integr. (VLSI) Syst.* **2009**, *17*, 627–637. [CrossRef]
138. Hande, A.; Polk, T.; Walker, W.; Bhatia, D. Indoor solar energy harvesting for sensor network router nodes. *Microprocess. Microsyst.* **2007**, *31*, 420–432. [CrossRef]
139. Li, W.; Lv, X.; Deng, Y.; Liu, J.; He, X. A review of non-isolated high step-up DC/DC converters in renewable energy applications. In Proceedings of the Twenty-Fourth Annual IEEE Applied Power Electronics Conference and Exposition, Washington, DC, USA, 15–19 February 2009; pp. 364–369.
140. Fu, L.; Zhang, X.; Guo, F.; Wang, J. A phase shift controlled current-fed quasi-switched-capacitor isolated dc/dc converter with GaN HEMTs for photovoltaic applications. In Proceedings of the IEEE Applied Power Electronics Conference and Exposition (APEC), Charlotte, NC, USA, 15–19 March 2015; pp. 191–198.
141. Sebald, G.; Guyomar, D.; Agbossou, A. On thermoelectric and pyroelectric energy harvesting. *Smart Mater. Struct.* **2009**, *18*, 125006. [CrossRef]
142. Sebald, G.; Lefeuvre, E.; Guyomar, D. Pyroelectric energy conversion: Optimization principles. *IEEE Trans. Ultrason. Ferroelectr. Freq. Control* **2008**, *55*, 538–551. [CrossRef]
143. Bowen, C.; Taylor, J.; Le Boulbar, E.; Zabek, D.; Topolov, V.Y. A modified figure of merit for pyroelectric energy harvesting. *Mater. Lett.* **2015**, *138*, 243–246. [CrossRef]
144. Shi, B.; Li, Z.; Fan, Y. Implantable energy-harvesting devices. *Adv. Mater.* **2018**, *30*, 1801511. [CrossRef]
145. Jain, A.; Bhullar, M.S. Emerging dimensions in the energy harvesting. *IOSR J. Electr. Electron. Eng.* **2012**, *3*, 70–80. [CrossRef]
146. Tsui, C.-Y.; Li, X.; Ki, W.-H. Energy harvesting and power delivery for implantable medical devices. *Found. Trends Electron. Des. Autom.* **2013**, *7*, 179–246. [CrossRef]
147. Khosropour, N.; Krummenacher, F.; Kayal, M. Fully integrated ultra-low power management system for micro-power solar energy harvesting applications. *Electron. Lett.* **2012**, *48*, 338–339. [CrossRef]
148. Ghosh, S.; Wang, H.-T.; Leon-Salas, W.D. A circuit for energy harvesting using on-chip solar cells. *IEEE Trans. Power Electron.* **2013**, *29*, 4658–4671. [CrossRef]
149. Peter, P.K.; Agarwal, V. On the input resistance of a reconfigurable switched capacitor DC–DC converter-based maximum power point tracker of a photovoltaic source. *IEEE Trans. Power Electron.* **2012**, *27*, 4880–4893. [CrossRef]
150. Chang, Y.-H.; Chen, C.-L.; Lin, T.-C. Reconfigurable switched-capacitor converter for maximum power point tracking of PV system. In Proceedings of the International MultiConference of Engineers and Computer Scientists, Hong Kong, China, 12–14 March 2014; pp. 791–796.
151. Wang, Y.; Luo, P.; Zheng, X.; Zhang, B. A 0.3 V–1.2 V ultra-low input voltage, reconfigurable switched-capacitor DC-DC converter for energy harvesting system. In Proceedings of the 13th IEEE International Conference on Solid State and Integrated Circuit Technology (ICSICT), Hangzhou, China, 25–28 October 2016; pp. 1333–1335.
152. D'hulst, R.; Sterken, T.; Puers, R.; Driesen, J. Requirements for power electronics used for energy harvesting devices. In Proceedings of the 5th International Workshop on Micro and Nanotechnology for Power Generation and Energy Conversion Application, Tokyo, Japan, 28–30 November 2005; pp. 53–56.
153. Rodič, M.; Milanovič, M.; Truntič, M.; Ošlaj, B. Switched-capacitor boost converter for low power energy harvesting applications. *Energies* **2018**, *11*, 3156. [CrossRef]
154. Chowdhury, I. Efficient Voltage Regulation Using Switched Capacitor DC/DC Converter from Battery and Energy Harvesting Power Sources. Ph.D. Thesis, University of Arizona, Tucson, AZ, USA, 17 September 2010.

155. Szarka, G.D.; Stark, B.H.; Burrow, S.G. Review of power conditioning for kinetic energy harvesting systems. *IEEE Trans. Power Electron.* **2012**, *27*, 803–815. [CrossRef]
156. Schamel, A.; Schmitz, P.; d'Annunzio, J.; Iorio, R. Ford C-Max plug-in hybrid. *MTZ Worldw.* **2013**, *74*, 4–10. [CrossRef]
157. Gray, T.; Shirk, M. 2010 Ford Fusion VIN 4757 hybrid electric vehicle battery test results. *Idaho Natl. Lab.* **2013**. [CrossRef]
158. Amjadi, Z.; Williamson, S.S. Advanced digital control for a switched capacitor and interleaved switched capacitor hybrid electric vehicle energy management system. *Int. J. Electr. Hybrid Veh.* **2011**, *3*, 272–292. [CrossRef]
159. Daowd, M.; Omar, N.; Bossche, P.V.D.; Van Mierlo, J. Capacitor based battery balancing system. *World Electr. Veh. J.* **2012**, *5*, 385–393. [CrossRef]
160. Cao, Y.; Lei, Y.; Pilawa-Podgurski, R.C.; Krein, P.T. Modular switched-capacitor dc-dc converters tied with lithium-ion batteries for use in battery electric vehicles. In Proceedings of the IEEE Energy Conversion Congress and Exposition (ECCE), Montreal, QC, Canada, 20–24 September 2015; pp. 85–91.
161. Zhang, Y.; Yao, C.; Wang, Z.; Chen, H.; He, X.; Zhang, X.; Li, H.; Wang, J. Development of a WBG-based transformerless electric vehicle charger with semiconductor isolation. In Proceedings of the IEEE 4th Southern Power Electronics Conference (SPEC), Singapore, 10–13 December 2018; pp. 1–6.
162. Kim, M.-Y.; Kim, C.-H.; Kim, J.-H.; Kim, D.-Y.; Moon, G.-W. Switched capacitor with chain structure for cell-balancing of lithium-ion batteries. In Proceedings of the IECON 2012, 38th Annual Conference on IEEE Industrial Electronics Society, Montreal, QC, Canada, 25–28 October 2012; pp. 2994–2999.
163. Elsayad, N.; Moradisizkoohi, H.; Mohammed, O. A new single-switch structure of a DC-DC converter with wide conversion ratio for fuel cell vehicles: Analysis and development. *IEEE J. Emerg. Sel. Top. Power Electron.* **2019**, *8*, 2785–2800. [CrossRef]
164. Maksimovic, D.; Dhar, S. Switched-capacitor DC-DC converters for low-power on-chip applications. In Proceedings of the 30th Annual IEEE Power Electronics Specialists Conference. Record (Cat. No. 99CH36321), Charleston, SC, USA, 1 July 1999; pp. 54–59.
165. Su, F.; Ki, W.-H.; Tsui, C.-Y. Regulated switched-capacitor doubler with interleaving control for continuous output regulation. *IEEE J. Solid State Circ.* **2009**, *44*, 1112–1120. [CrossRef]
166. Carvalho, C.; Paulino, N. A MOSFET only, step-up DC-DC micro power converter, for solar energy harvesting applications. In Proceedings of the17th International Conference Mixed Design of Integrated Circuits and Systems-MIXDES, Wroclaw, Poland, 24–26 June 2010; pp. 499–504.
167. Carvalho, C.; Oliveira, J.P.; Paulino, N. Survey and analysis of the design issues of a low cost micro power dc-dc step up converter for indoor light energy harvesting applications. In Proceedings of the19th International Conference Mixed Design of Integrated Circuits and Systems-MIXDES, Warsaw, Poland, 24–26 May 2012; pp. 455–460.
168. Ying, T.; Ki, W.-H.; Chan, M. Area-efficient CMOS charge pumps for LCD drivers. *IEEE J. Solid State Circ.* **2003**, *38*, 1721–1725. [CrossRef]
169. Lin, Y.-C.; Luo, Y.-K.; Chen, K.-H.; Hsu, W.-C. Liquid crystal display (LCD) supplied by highly integrated dual-side dual-output switched-capacitor DC-DC converter with only two flying capacitors. *IEEE Trans. Circ. Syst. I Regul. Pap.* **2011**, *59*, 439–446. [CrossRef]
170. Stala, R. The switch-mode flying-capacitor DC–DC converters with improved natural balancing. *IEEE Trans. Ind. Electron.* **2010**, *57*, 1369–1382. [CrossRef]
171. Fan, S.; Dong, J.; Zhang, R.; Xue, Z.; Geng, L. A reconfigurable multi-ratio charge pump with wide input/output voltage range for wireless energy harvesting system. In Proceedings of the IEEE MTT-S International Wireless Symposium (IWS), Chengdu, China, 6–10 May 2018; pp. 1–3.
172. Kamel, M.H.; Abdelmagid, B.A.; Mohieldin, A.N. A fully-integrated efficient power management system for micro-scale biomedical applications. In Proceedings of the IEEE 29th International Symposium on Industrial Electronics (ISIE), Delft, The Netherlands, 17–19 June 2020; pp. 394–399.
173. Wu, J.-T.; Chang, K.-L. MOS charge pumps for low-voltage operation. *IEEE J. Solid State Circ.* **1998**, *33*, 592–597.
174. Witters, J.S.; Groeseneken, G.; Maes, H.E. Analysis and modeling of on-chip high-voltage generator circuits for use in EEPROM circuits. *IEEE J. Solid State Circ.* **1989**, *24*, 1372–1380. [CrossRef]
175. Palumbo, G.; Pappalardo, D.; Gaibotti, M. Charge pump with adaptive stages for non-volatile memories. *IEE Proc. Circ. Devices Syst.* **2006**, *153*, 136–142. [CrossRef]
176. Lu, Y.; Ki, W.-H.; Yue, C.P. An NMOS-LDO regulated switched-capacitor DC–DC converter with fast-response adaptive-phase digital control. *IEEE Trans. Power Electron.* **2015**, *31*, 1294–1303. [CrossRef]
177. Cho, T.B.; Gray, P.R. A 10-bit, 20-MS/s, 35-mW pipeline A/D converter. In Proceedings of the IEEE Custom Integrated Circuits Conference (CICC) 1994, San Diego, CA, USA, 1–4 May 1994; pp. 499–502.
178. Ueno, F.; Inoue, T.; Oota, I.; Harada, I. Emergency power supply for small computer systems. In Proceedings of the IEEE International Sympoisum on Circuits and Systems, Singapore, 11–14 June 1991; pp. 1065–1068.
179. Su, F.; Ki, W.-H. An integrated reconfigurable sc power converter with hybrid gate control scheme for mobile display driver applications. In Proceedings of the IEEE Asian Solid State Circuits Conference, Fukuoka, Japan, 3–5 November 2008; pp. 169–172.
180. Su, F.; Ki, W.-H. Component-efficient multiphase switched-capacitor DC–DC converter with configurable conversion ratios for LCD driver applications. *IEEE Trans. Circ. Syst. II Express Briefs* **2008**, *55*, 753–757.

181. Tong, T.; Lee, S.K.; Zhang, X.; Brooks, D.; Wei, G.-Y. A fully integrated reconfigurable switched-capacitor DC-DC converter with four stacked output channels for voltage stacking applications. *IEEE J. Solid State Circ.* **2016**, *51*, 2142–2152. [CrossRef]
182. Sanders, S.R.; Alon, E.; Le, H.-P.; Seeman, M.D.; John, M.; Ng, V.W. The road to fully integrated DC–DC conversion via the switched-capacitor approach. *IEEE Trans. Power Electron.* **2013**, *28*, 4146–4155. [CrossRef]
183. Fan, Z.; Lei, D.; Peng, F.Z.; Zhaoming, Q. A new design method for high efficiency DC-DC converters with flying capacitor technology. In Proceedings of the Twenty-First Annual IEEE Applied Power Electronics Conference and Exposition (APEC), Dallas, TX, USA, 19–23 March 2006; p. 5.
184. Texas Instruments. MAX660 Switched Capacitor Voltage Converter. Available online: http://www.ti.com/lit/ds/symlink/max660.pdf (accessed on 1 March 2021).
185. Texas Instruments. LM2660 Switched Capacitor Voltage Converter. Available online: http://www.ti.com/lit/ds/symlink/lm2660.pdf?ts=1590365124686 (accessed on 1 March 2021).
186. National Semiconductor. LM2685 Dual Output Regulated Switched Capacitor Voltage Converter. Available online: http://www.farnell.com/datasheets/78611.pdf (accessed on 1 March 2021).
187. Maxim Integrated. 125mA, Frequency-Selectable, Switched-Capacitor Voltage Converters. Available online: https://www.maximintegrated.com/en/products/power/charge-pumps/MAX1681.html (accessed on 1 March 2021).
188. Maxim Integrated. MAX860/MAX861 50mA, Frequency-Selectable, Switched-Capacitor Voltage Converters. Available online: https://datasheets.maximintegrated.com/en/ds/MAX860-MAX861.pdf (accessed on 1 March 2021).
189. Texas Instruments. LT1054 Switched-capacitor Voltage Converters with Regulators. Available online: http://www.ti.com/lit/ds/symlink/lt1054.pdf?ts=1590365080642. (accessed on 1 March 2021).
190. Texas Instruments. LM2665 Switched Capacitor Voltage Converter. Available online: http://www.ti.com/lit/ds/symlink/lm2665.pdf (accessed on 1 March 2021).
191. Texas Instruments. LM2767 Switched Capacitor Voltage Converter. Available online: https://www.ti.com/product/LM2767 (accessed on 1 March 2021).
192. Analog Devices. 320 mA Switched Capacitor Voltage Doubler. Available online: https://www.analog.com/media/en/technical-documentation/data-sheets/ADP3610.pdf (accessed on 1 March 2021).
193. Microchip. TCM 828 Switched Capacitor Voltage Converters. Available online: http://ww1.microchip.com/downloads/en/DeviceDoc/21488b.pdf (accessed on 1 March 2021).